END
DATE
FILMED
8-83
DTIC

MICROCOPY RESOLUTION TEST CHART

NATIONAL BUREAU OF STANDARDS - 1963 - A

⑫

REPORT DOCUMENTATION PAGE		READ INSTRUCTIONS BEFORE COMPLETING FORM
1. REPORT NUMBER NR 092-545/2/83	2. GOVT ACCESSION NO. AD-A130915	3. RECIPIENT'S CATALOG NUMBER
4. TITLE (and Subtitle) THE PHOTODISSOCIATION OF NITROMETHANE AT 193 NM		5. TYPE OF REPORT & PERIOD COVERED Technical
		6. PERFORMING ORG. REPORT NUMBER
7. AUTHOR(s) L. J. Butler, D. Krajnovich, Y.T. Lee, G. Ondrey and R. Bersohn		8. CONTRACT OR GRANT NUMBER(s) N00014-75-C-0671 NR 092-545
9. PERFORMING ORGANIZATION NAME AND ADDRESS Professor Y. T. Lee Dept. of Chemistry, University of California Berkeley, California 94720		10. PROGRAM ELEMENT, PROJECT, TASK AREA & WORK UNIT NUMBERS
11. CONTROLLING OFFICE NAME AND ADDRESS Dr. Richard Miller, Office of Naval Research Department of the Navy, Code 613A:MAK 800 N. Quincy Street, Arlington, VA 22217		12. REPORT DATE February 28, 1983
		13. NUMBER OF PAGES 65
14. MONITORING AGENCY NAME & ADDRESS(if different from Controlling Office) Office of Naval Research Resident Representative University of California, 239 Campbell Hall Berkeley, California 94720		15. SECURITY CLASS. (of this report) UNCLASSIFIED
		15a. DECLASSIFICATION/DOWNGRADING SCHEDULE

16. DISTRIBUTION STATEMENT (of this Report)

Unlimited

17. DISTRIBUTION STATEMENT (of the abstract entered in Block 20, if different from Report)

DTIC
SELECTE
AUG 0 2 1983
E

18. SUPPLEMENTARY NOTES

Submitted for publication in the Journal of Chemical Physics.

19. KEY WORDS (Continue on reverse side if necessary and identify by block number)

Photodissociation of nitromethane at 193 nm.
Molecular beam photofragmentation of nitromethane.
Photofragmentation dynamics of nitromethane.

20. ABSTRACT (Continue on reverse side if necessary and identify by block number)

The dissociation of nitromethane following the excitation of the $\pi^* \leftarrow \pi$ transition at 193 nm has been investigated by two independent and complementary techniques, product emission spectroscopy and molecular beam photofragment translational energy spectroscopy. The primary process is shown to be cleavage of the C-N bond to yield CH_3 and NO_2 radicals. The translational energy distribution for this chemical process indicates that there are two distinct mechanisms by which CH_3 and NO_2 radicals are

DD $_{1 \ JAN \ 73}^{FORM}$ 1473 EDITION OF 1 NOV 65 IS OBSOLETE
S/N 0102-LF-014-6601

20. Abstract (Continued)

produced. The dominant mechanism releasing a relatively large fraction of the total available energy to translation probably gives NO_2 radicals in a vibrationally excited $^2B_2$ state. When dissociated, other nitroalkanes exhibit the same emission spectrum as CH_3NO_2, suggesting little transfer of energy from the excited NO_2 group to the alkyl group during dissociation for the dominant mechanism. This conclusion is supported by the apparent loss of the slow NO_2 product in the molecular beam studies to unimolecular dissociation to $NO + O$, which will occur for NO_2 with 72 kcal/mole or more internal energy.

Evidence is presented which suggests that the NO_2 produced via the minor mecnanism, which releases a smaller fraction of the available energy to translation, has a large cross section for absorbing an additional photon via a parallel transition and dissociating to $NO + O$.

THE PHOTODISSOCIATION OF NITROMETHANE AT 193 nm

L. J. Butler, D. Krajnovich and Y. T. Lee
Materials and Molecular Research Division
Lawrence Berkeley Laboratory and
Department of Chemistry
University of California
Berkeley, California 94720

and

G. Ondrey and R. Bersohn
Department of Chemistry
Columbia University
New York, New York 10027

February 1983

ABSTRACT

The dissociation of nitromethane following the excitation of the $\pi^* \leftarrow \pi$ transition at 193 nm has been investigated by two independent and complementary techniques, product emission spectroscopy and molecular beam photofragment translational energy spectroscopy. The primary process is shown to be cleavage of the C-N bond to yield CH_3 and NO_2 radicals. The translational energy distribution for this chemical process indicates that there are two distinct mechanisms by which CH_3 and NO_2 radicals are produced. The dominant mechanism releasing a relatively large fraction of the total available energy to translation probably gives NO_2 radicals in a vibrationally excited $^2B_2$ state. When dissociated, other nitroalkanes exhibit the same emission spectrum as CH_3NO_2, suggesting little transfer of energy from the excited NO_2 group to the alkyl group during dissociation for the dominant mechanism. This conclusion is supported by the

apparent loss of the slow NO_2 product in the molecular beam studies to unimolecular dissociation to $NO + O$, which will occur for NO_2 with 72 kcal/mole or more internal energy.

Evidence is presented which suggests that the NO_2 produced via the minor mechanism, which releases a smaller fraction of the available energy to translation, has a large cross section for absorbing an additional photon via a parallel transition and dissociating to $NO + O$.

INTRODUCTIUN

The optical absorption spectrum of nitromethane[1,2] is a broad continuum extending down from 370 nm to the vuv having maxima at 198 nm (ϵ = 4000 M^{-1} cm^{-1}) and 270 nm (ϵ = 10 M^{-1}). Nagakura[2] assigned the strong and weak banos to $\pi^* \leftarrow \pi$ and $\pi^* \leftarrow n$ transitions respectively, where both transitions are localized on the NO_2 moiety. Photoelectron and electron energy loss spectroscopic studies[3-5] are for the most part consistent with these assignments although Rabelais[3] believes the strong transition to be a promotion of a C–N σ bonoing electron to the antibonding π^* orbital of the NO_2 and Flicker et al.[5] suggest tnat this $\pi^* \leftarrow \sigma$ transition occurs in the same region as the $\pi^* \leftarrow n$ transition and accounts for almost all of the 270 nm peak in the optical spectrum.

The energetically allowed photodissociation channels involving simple oond rupture, and two other channels involving the migration of H or O atoms, are shown in Fig. 1. A short review of previous studies of the ultraviolet photolysis of nitromethane has been presented by Schoen et al.[6] Gas pnase photochemical studies to date have been limited to excitation of the $\pi^* \leftarrow n$ transition (perhaps better assigned as a $\pi^* \leftarrow \sigma$ transition by Flicker et al.). Flash photolysis studies[7,8] indicate that formation of CH_3 and NO_2 radicals is the major process for this region, though Honda et al.[7] show evidence of other minor cnannels.

Three recent gas phase photodissociation studies in the region of the 270 nm transition(s) have relied on direct aetection of the photodissociation proaucts[9,10,6] by laser induced fluorescence (LIF) or electron bombardment ionization methods. Spears ana Brugge[9] dissociated CH_3NO_2

at 252.6 nm and probed the vibrational population of the ground electronic state NO_2 formed. By filtering the LIF signal they concluded that the NO_2 is highly excited in all vibrational modes. Kwok et al.[10] studied the photodissociation of nitromethane at 266 nm in a collision-free crossed laser-molecular beam experiment with mass spectrometric detection. Although the vibrational predissociation of small clusters of nitromethane molecules was detected, dissociation products from the monomer were not observed. They estimated from their detection sensitivity and the absorption cross section at 266 nm that the quantum yield for dissociation of the monomer is less than 3 percent for several possible products that would fragment to give CH_3^+, NO_2^+, NO^+, HNO^+, or CH_3NO^+ in the ionizer. Schoen et al.[6] used a 5 ps photolyzing pulse at 264 nm and monitored the subsequent evolution of the NO_2 fragment by LIF with a 5 ps 527 nm pulse. They estimated a 1 percent quantum yield of NO_2 product. They found that the dissociation occurred in <5 ps and that some of the NO_2 product was formed in an excited fluorescing state.

In the present paper, two complementary techniques have been used to study the primary processes occurring when nitromethane is excited at 193 nm near the maximum of the $\pi^* \leftarrow \pi$ transition. The method of photofragment translational energy spectroscopy in a crossed laser-molecular beam apparatus identifies the primary photochemical process as cleavage of the C-N bond and shows that there are two distinct mechanisms which produce CH_3 and NO_2 products. Product translational energy distributions for the dissociation pathways are measured and a comparison of the product velocity distributions suggest that for the dominant process the NO_2 radical retains much of the internal energy. The method of fluorescence

emission spectroscopy identifies the excited electronic state of the NO_2 radical for the dominant process and the emission spectra of a series of nitroalkanes provides independent evidence that little energy has transferred from the NO_2 group to the CH_3 during dissociation. The emission spectra suggest and the molecular beam studies confirm that the hottest $NO_2(^2B_2)$ is formed with sufficient internal energy to spontaneously decompose. Evidence from the molecular beam studies is also presented which suggests that the NO_2 produced in the minor primary processes undergoes efficient secondary photodissociation to $NO + O$ via a parallel transition.

EXPERIMENTAL

The fluorescence emission studies and the laser polarization dependence measurement presented here were done at Columbia University while the complementary molecular beam study presented was done at Berkeley. The results of these independent measurements when combined allowed many conclusions to be made about the primary photochemical processes studied here. Some product velocity distributions were measured at Columbia, but the Berkeley data is presented as it is more complete and as the Berkeley apparatus has a rotatable detector and is thus sensitive to lower product recoil energies than the fixed 90° geometry detector at Columbia.

A. Molecular Beam Experiments

Time-of-flight (TOF) and angular distributions of the photofragments were measured in a molecular beam apparatus described in detail elsewhere.[11] The molecular beam was formed by bubbling helium through nitromethane (Mallinckrodt spectrophotometric grade) maintained at 20°C and expanding the mixture through a 0.005" diameter stainless steel nozzle at a total stagnation pressure of 300 torr (11 percent CH_3NO_2/89 percent He). The nozzle was heated to 240°C to effectively eliminate contributions from molecular clusters in the beam. The velocity distribution of the nitromethane beam was determined by time-of-flight measurements. The beam had a peak velocity of 1470 m/s with the full width at half maximum (FWHM) of the distribution being 18 percent. The beam was collimated by a skimmer, and, after passing through two pressure reducing differential chambers, it was crossed by the laser beam. The molecular beam was defined to an angular divergence of ~1.6°.

The 193 nm photons were produced by a Lambda Physik EMG 101 ArF excimer laser. For most of the data taken for measurement of product translational energy and angular distributions, the laser was run at a repetition rate of 50 Hz and the average power was maintained at 2.0 ± 0.04 W (40 mJ/pulse). The laser light was unpolarized and was focussed onto the molecular beam by a 35 cm focal length fused silica spherical lens to a final spot size of ~4 mm^2. This resulted in a (time-integrated) photon flux through the interaction region with the molecular beam on the order of ~1 x 10^{18} photons/cm^2-pulse. For the power dependence measurements, the power was adjusted by changing the high voltage for the gas discharge and running the laser with the beginning or end of a gas fill; the focus and alignment were kept constant.

The dissociation products were detected in the plane of the laser and molecular beams by a rotatable ultra-high vacuum mass spectrometer consisting of an electron bombardment ionizer, quadrupole mass filter, and particle counter. The flight path between the beam crossing point and the ionizer was 20.8 cm. Angular and TOF distributions were measured in the usual way.[12]

Signal was observed when the quadrupole mass spectrometer was set to pass the following mass to charge ratios: m/e = 46, 30, 16, 15, 14, and 13 corresponding to NO_2^+, NO^+, O^+, CH_3^+, (CH_2^+, N^+), and CH^+. Typical signal levels at a detector angle of 10° from the molecular beam were 2.8 counts/pulse for NO^+, 0.18 counts/pulse for NO_2^+, 0.85 counts/pulse for O^+, and 0.42 counts/pulse for CH_3^+. The NO_2^+ signal was much lower than the NO^+ signal from the NO_2 product presumably due to extensive fragmentation of vibrationally hot NO_2 molecules in the

ionizer. No significant signal was observed at m/e = 47, 45, 44, 31 or 29 corresponding to $HONO^+$, CH_3NO^+, CH_2NO^+, (CH_3O^+, HNO^+), and (CH_3N^+, CHO^+) respectively. At all masses but m/e = 29, this signal was less than 1 percent of the NO^+ signal level. At m/e = 29 a signal on the order of 10 percent of the NO^+ signal was observed and was attributed to crosstalk from the large signal at m/e = 30 due to the finite resolution of the quadrupole.

TOF distributions were measured for CH_3^+, NO_2^+, and NO^+ at three detector angles with respect to the molecular beam: 10°, 25°, and 40°. TOF data was also taken for O^+ at 10° at the same photon flux as the above data (noted previously) and for m/e = 14 and 13 at 10° and laser pulse energies of ~ 13 mJ. The data presented for CH_3^+, NO_2^+, NO^+, and O^+ were obtained by counting for between 5×10^4 and 10^6 laser pulses at each angle. All but one of the CH_3^+ TOF spectra taken had a very slow laser correlated background arriving between 210 and 750 μsec that remained when the laser beam was pulsed but the molecular beam was flagged.[13] It did not significantly overlap the data and was discriminated against in the angular distribution measurements described below.

Angular distributions were measured for CH_3^+, NO_2^+, and NO^+ between 8° and 45° in 3° increments, although good signal to noise ratios were not obtained for NO_2^+. We gated the CH_3^+ signal from 20 - 200 μsec, so that the slow laser-correlated background was not included, and corrected for this in our calculation for the fit to the angular distribution. Each point in the CH_3^+ angular distribution is the integrated signal for 12,000 laser shots and is the normalized sum of a forward/backward angular

scan. The NO^+ angular disribution is the sum of three scans taken by reversing airections in between each; each point is the integrated signal collected for 6,000 laser pulses.

b. Laser Polarization Dependence

The dependence of the m/e = 15, CH_3^+, signal on the polarization of the laser was performed with a low photon flux on the Columbia molecular beam apparatus described elsewhere.[14] The product was detected 7.8 cm from the interaction region at right angles to the pulsea laser and an effusive molecular beam. Here the laser was focussea with a 40 cm focal length cylindrical lens and polarized with a pile of ten plates polarizer, resulting in a photon flux of $\sim 1 \times 10^{17}$ photons/cm^2. The electric vector of the lignt was rotatea with a half wave plate cut for 193 nm (Optics for Research). The TUF distribution for m/e = 15 was measurea at eight different polarization angles in a staggerea fasnion to average out experimental fluctuations in background signal and laser power. The laser power was kept constant to within 15 percent ana signal was accumulatea for 2160 laser snots at each angle.

C. Fluorescence Emission Experiments

Fluorescence measurements were carried out in a flowing cell. Pressures rangea from 20 to 100 mtorr and were regulated to within 2 percent. Because of the broad spectral range of the emission, several photomultipliers were usea. The fluorescence from the dissociation of nitromethane was viewed with an RCA 31035 photomultiplier tube which was coolea with dry ice/acetone. This PMT has a flat response from 400 to

800 nm, so the spectrum (Fig. 6), gives a true picture of the NO_2^* emission. For comparison witn different molecules (Fig. 7) uncorrected spectra were recorded trom 380 to 650 nm. The resolution of tne 1/4 m monochromator (Jarrell-Ash) was ~4 nm FWHM.

RESULTS AND ANALYSIS

A.   Determination of the Primary Photodissociation Processes

There is strong evidence from the molecular beam study that CH_3 is the only primary carbon containing photodissociation fragment. The TOF spectra of m/e = 15 corresponding to CH_3^+ is shown in Fig. 2. The m/e = 13, CH^+, TOF data is exactly the same as the CH_3^+ data when the usual small correction for the mass dependent ion flight time through the mass spectrometer is made. This suggests that CH^+ is a daughter ion of CH_3 and that there are no other primary products which give CH^+ in the ionizer. In addition, no significant signal (<1 percent of the NO^+ signal or signal accounted for by crosstalk from m/e = 30 due to the finite resolution of the quadrupole) was observed at the masses corresponding to $HONO^+$, CH_3NO^+, CH_2NO^+, (CH_3O^+, HNO^+), or (CH_3N^+, CHO^+). These observations also support the conclusion that the CH_3 radical is the only primary carbon containing photofragment and thus identifies the primary chemical process as:

$$CH_3NO_2 \rightarrow CH_3 + NO_2 . \tag{1}$$
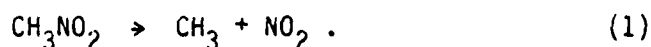
The angular distribution of the m/e = 15, CH_3^+, signal is shown in Fig. 3. The angular and TOF distributions of the methyl product were fit by a trial-and-error forward convolution method using different assumed forms for the center-of-mass (c.m.) translational energy distribution, $P(E')$, and angular distribution, $w(\theta)$. For a single photon process in the electric dipole approximation, tne c.m. angular distribution must be of the form

$$w(\theta) = 1/4\pi[1 + 2bP_2(\cos\theta)], \qquad\qquad (2)$$

where θ is the angle between the electric vector of the laser light and the final c.m. recoil direction of the products, and the anisotropy parameter, b, is constrained to the range $-0.5 \le b \le +1.0$. Therefore, the c.m. angular distribution is completely described by the single parameter b. A completely flexible point form for the P(E') was used. The fits to the CH_3^+ data in Figs. 2 and 3 were calculated using the solid-line P(E') in Fig. 4 and assuming an isotropic c.m. angular distribution (i.e., b = 0). We then attempted to fit the data with several anisotropy parameters between b = 0.0 and b = -0.5. The fit to the laboratory angular distribution can be improved if b = -0.1 is used, but it begins to degrade the best simultaneous 10°, 25°, and 40° TOF fits. With a b parameter of -0.3 it is impossible to get an acceptable fit to the TOF's or angular distribution. The result of the analysis is that if the entire primary photodissociation process is fit with one anisotropy parameter, it must be nearly isotropic in the c.m. reference frame. The nearly isotropic distribution observed at this laser energy fluence may have been influenced by saturation effects. The photon flux in this experiment is high enough to dissociate almost all the molecules regardless of the orientation of their transition moment with respect to the polarization of the laser. For a perhaps more significant measurement of the anisotropy parameter, see Part D.

It is important to note that though the laser used in this experiment was unpolarized, the data is still sensitive to anisotropy as a consequence of the geometry of our detection. The laser light can be resolved into a

component perpendicular to the plane of the laser and molecular beam, the plane of detection, and an equal component parallel to the molecular beam. The perpendicular component gives an isotropic contribution to the detection plane but the parallel component does not.

The translational energy distribution for the primary photochemical process, process (1), is shown by the solid line in Fig 4. Derived from the CH_3^+ TOF data, it has two maxima, a sharp feature peaking at 2 kcal/mole translational energy and a broad feature peaking at 8 kcal/mole and extending out to 44 kcal/mole in translation. Within the resolution of this experiment, the shape indicates that there are two distinct physical mechanisms by which the chemical products CH_3 and NO_2 are produced. A minor mechanism releases a small fraction of the total available energy to translation and peaks at 2 kcal/mole and the dominant mechanism channels a larger amount of the total available energy to translation and extends out to a translational energy of 44 kcal/mole.

B. Fluorescence Emission from NO_2^* Product

A prompt fluorescence was seen after the excimer laser was fired through a cell containing 20 mtorr of nitromethane. The fluorescence lifetime was measured to be 35 ± 5 µs (Fig. 5). In the Discussion Section it will be suggested that this is characteristic of the $^2B_2$ state of NO_2. The dispersed fluorescence is shown in Fig. 6 for nitromethane. The emission extends from the dissociation limit of NO_2 (398 nm) out to the infrared, with a complete lack of any structural features. Similar broad spectra, characteristic of NO_2, have been reported for the chemiluminescent

reaction of $O + NO$[15] and the photodissociation of $(NO_2)_2$.[16] The presence of emission near the dissociation limit of NO_2 indicates that some of the NO_2 product may have been formed with enough internal energy to unimolecularly dissociate to $NO + O$, as is discussed in part C.

As shown in Fig. 7, variations in the alkyl group attached to NO_2 do not influence the emission spectrum. This result implies that the excited state NO_2 is formed in the same set of final states regardless of the alkyl group and that the dissociation time is faster than the time necessary for relaxation of the NO_2 by the alkyl groups.

Figure 8 shows the emission spectrum obtained when nitromethane was photolyzed with the laser strongly focussed. Superimposed on the NO_2^* continuum are additional features due to $CN(B \rightarrow X)$ and $CH(A \rightarrow X)$ emission which can only arise from a multiphoton process.

C. Spontaneous Unimolecular Decay of Highly Excited NO_2

The $m/e = 46$, NO_2^+, TOF data is shown in Fig. 9. As CH_3 and NO_2 are formed in the primary dissociation, their velocities with respect to the center of mass are related by momentum conservation. One should be able to fit the NO_2^+ TOF data using the $P(E')$ which fit the CH_3^+ TOF data. When we attempted to do this we found that the fast NO_2 product was correctly related to the fast CH_3 product by momentum conservation, but that much of the slow NO_2 product was not detected. The good fits to the NO_2^+ data in Fig. 9 were actually calculated from the dashed-line $P(E')$ in Fig. 4 (again assuming $b = 0$). Evidently, much of the NO_2 product formed in dissociation events releasing less than 16 kcal/mole to translation has disappeared. We will now consider what evidence we have concerning how this NO_2 is lost.

The NO_2^* fluorescence emission studies of part B have shown that the excess energy is concentrated in the excited NO_2 product. Because the band origin of the $^2B_2$ state is calculated to be 27.9 kcal/mole[17,18] and the total available energy is 90 kcal/mole, any NO_2 from dissociation events releasing 62 kcal/mole or less into translation could be in the $^2B_2$ state. Thus we tentatively assign the major primary dissociation process (corresponding to the broad energy distribution extending out to 44 kcal/mole) to process (3) below:

$$CH_3NO_2 \longrightarrow CH_3 + NO_2(^2B_2) \qquad (3)$$
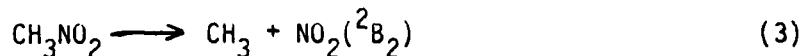
It appears from the P(E') derived from the NO_2 TOF's that all of the surviving NO_2 results from this process. The P(E') derived from the NO_2^+ data starts to deviate from the P(E') derived from the CH_3^+ data below 16 kcal/mole. At 16 kcal/mole translational energy, the NO_2 product could have as much as 74 kcal/mole internal energy. With 72 kcal/mole or more internal energy, $NO_2(^2B_2)$ will unimolecularly dissociate to NO + O. Thus the loss of some of the $NO_2(^2B_2)$ product at translational energies less than 16 kcal/mole might reasonably be assigned to its unimolecular dissociation to NO + O (process 4 below), particularly as the $NO_2(^2B_2)$ fluorescence extends to the dissociation limit.

$$CH_3NO_2 \rightarrow CH_3 + NO_2 \qquad (4)$$
$$ \longrightarrow NO + O$$
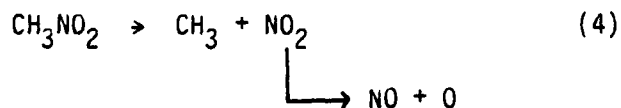
Now notice that practically all of the NO_2 formed in the minor primary dissociation process (which gives rise to the peak in the CH_3^+ P(E') at 2 kcal/mole) has also been lost. Whether this should be ascribed to the unimolecular dissociation of this NO_2 product is much less clear. If this were so, then essentially all of this NO_2 would have had to retain 72 kcal/mole or more internal energy, since there is no hint of the 2 kcal/mole feature in the NO_2 product P(E'). Analysis of the NO^+ and O^+ data in the following subsection suggests that, for some reason, the NO_2 formed in the minor primary process undergoes very efficient secondary photodissociation to NO + O.

D. Secondary Photodissociation of NO_2

The NO^+ TOF distributions are shown in Fig. 10. They are not identical to the NO_2^+ distributions shown in Figure 9. Therefore the NO^+ signal is not due solely to cracking of NO_2 in the ionizer.[19] The most striking difference between NO^+ and NO_2^+ is the presence of a fast "shoulder" in the NO^+ TOF distributions. This shoulder becomes quite prominent at larger angles. Also, the main peak in the NO^+ distribution is slightly broader than in the NO_2^+ distribution.

Initially we thought that the shoulder and broadening in the NO^+ data might be entirely due to NO radicals produced in the spontaneous unimolecular decay of hot NO_2 (see Part C). Certainly the slight broadening of the main peak in the NO^+ TOF distribution at small angles may be attributed to this cause. However, for energy and momentum to be conserved spontaneous decay of hot NO_2 cannot account for the fast shoulder in the NO^+ TOF

distributions. At 10°, the fastest product in the shoulder is travelling at 2.5×10^5 cm/s in the c.m. frame. In a sequential dissociation of CH_3NO_2 producing $CH_3 + NO + O$, the NO will attain a maximum velocity for a given amount of translational energy when the CH_3 and O are formed moving in the opposite direction of the NO with the same speed. For 18 kcal/mole available translational energy, the maximum NO velocity is calculated to be only 1.6×10^5 cm/sec. This maximum NO velocity is still much too slow to account for the fastest observed NO^+ product.

Another explanation for the fast NO^+ signal is that secondary photodissociation of the NO_2 product is occurring during the excimer laser pulse:

$$NO_2 \xrightarrow{\text{193 nm}} NO + O. \tag{5}$$

To test this explanation we measured an O^+ TOF distribution at 10° (Fig. 11). The shoulder on the O^+ distribution begins at even shorter times than the shoulder on the NO^+ TOF distribution, as expected on the basis of reaction (5). (Of course, the O^+ shoulder may contain contributions from both NO and O, but the contribution from O will dominate the fastest part of the shoulder.)

While this evidence convinced us that rxn. (5) is occurring under our experimental conditions, it is clear that not all of the NO_2 undergoes secondary photodissociation. A lot of NO_2 survives. In fact, the experimental $CH_3:NO_2$ ratio (calculated by correcting the measured CH_3^+ and NO^+ signals for relative ionization cross sections and

radical fragmentation in the ionizer) agrees with the CH_3:NO_2 ratio calculated from the CH_3 and NO_2 P(E')'s in Fig. 4 within experimental error. (The details of this calculation are given in Appendix I). That is, the majority of the "missing" NO_2 seems to be accounted for already by the discrepancy between the CH_3 and NO_2 P(E')'s. This would seem to indicate that only a rather small fraction of the NO_2 corresponding to the NO_2 P(E') undergoes secondary photodissociation. If this is the case, the intensities of the shoulders in the NO^+ and O^+ TOF's, relative to the main peak, should decrease linearly as the laser power is decreased.[20]

Even before we measured the O^+ TOF distribution, we remeasured the NO^+ TOF distribution at a laser power ten times lower than that used in Fig. 10. (This measurement was only made at $\Theta = 40°$, where the shoulder is more prominent.) To our surprise, the shoulder intensity relative to the main peak was only slightly (~20 percent) lower, compared to the ~10-fold change which had been anticipated. After measuring the O^+ TOF distribution, and convincing ourselves that secondary NO_2 photodissociation had to be occurring, we repeated the NO^+ TOF measurements at three laser powers spanning a 50-fold range. The raw data is shown in Fig. 12, where all three distributions have been normalized to the same peak height. The dependence of the relative shoulder intensity on the laser power is confirmed, but the power dependence is indeed very weak.

To obtain a measure of the relative shoulder intensity, we calculated the ratio of the signal in the shoulder (channels 15-35) to the signal in the main peak (channels 36-120). The background/channel was calculated by averaging channels 2-13 and was subtracted out before integrating the TOF

distributions. The dwell time per channel was 3 µs. The results for the three measurements of Fig. 12, as well as for the two earlier measurements, are collected in Table 1. As the laser pulse energy increases from 0.7 to 33 mJ/pulse, a factor of 47, the relative shoulder intensity increases by only a factor of 1.5. For reference, the <u>total</u> NO^+ signal increases by a factor of six over this same range.

We are faced with an apparent paradox. The weak power-dependence of the shoulder intensity indicates that the secondary photodissociation signal is strongly saturated, just as the primary nitromethane photodissociation signal is strongly saturated. Yet the measured $CH_3:NO_2$ signal ratio indicates that most of the NO_2 primary product survives (Appendix I). The most reasonable way out of this dilemma is to attribute the secondary photodissociation signal to NO_2 which is produced in the minor primary photodissociation process which gives rise to the "blip" in the CH_3 $P(E')$ at low recoil energies. We should emphasize that very hot NO_2 $(^2B_2)$ from the major primary photodissociation process cannot contribute to the secondary photodissociation signal, since NO_2 $(^2B_2)$ levels which lie above the NO $(^2\pi)$ + $O(^3P)$ limit are strongly predissociated (predissociation lifetimes on the order of picoseconds), and would not live long enough to absorb a second photon. This also implies that most of the NO_2 which is produced in the minor primary process, while presumably vibrationally hot, must be below the $NO(^2\pi)$ + $O(^3P)$ limit.

On the basis of the above assignment, we attempted to fit the NO^+ and O^+ data by varying the $P(E')$ and anisotropy parameter for the secondary photodissociation reaction (5) and the ratio, ϵ, of the fraction of NO_2

which undergoes secondary photodissociation to the fraction of surviving NO_2. The details of the calculations and the final fits are given in Appendix II (see Figs. 14-17). Here we will only mention the main results. (1) To fit the shape of the shoulders in the NO^+ TOF distributions, it was necessary to use a $P(E')$ for reaction (5) which peaked around 10 kcal/mole and tailed off smoothly to zero around 100 kcal/mole, with a mean translational energy of 31 kcal/mole. (2) To fit the relative shoulder intensities in the NO^+ TOF's at $10°$, $25°$ and $40°$, it was necessary to use a positive anisotropy parameter ($b = +0.5$) for reaction (5). Evidently, the secondary photodissociation of NO_2 proceeds via a parallel transition. (3) To fit the observed ratio of the shoulder intensity to the main peak in the NO^+ and O^+ TOF's, it was necessary to assume that $\epsilon \sim 0.50$. This implies that about 1/3 of the total NO_2 (less that fraction which spontaneously decomposes) undergoes secondary photodissociation at our highest laser pulse energies. For discussion of the quantitative significance of the derived ϵ value, see Appendix II.

To summarize, we have assumed that the NO_2 which is produced via the minor photodissociation channel of CH_3NO_2 (which gives rise to the blip in the CH_3 $P(E')$) undergoes very efficient secondary photodissociation to $NO + O$, while the NO_2 ($^2B_2$) which is produced in the major primary photodissociation process does not. On the basis of this assumption, we have been able to calculate very good fits to all of the NO^+ and O^+ data and at the same time rationalize (roughly) the observed percentage of NO_2 undergoing secondary photodissociation and the very weak power-dependence of the secondary photodissociation signal.

E.   Polarization Dependence Measurement

The dependence of the CH_3^+ signal on the polarization of tne laser was measurea at the lower pnoton flux of $\sim 1 \times 10^{17}$ photons/cm^2 in the effusive molecular beam apparatus. Tne result was an anisotropic distribution shown in Fig. 13. Each point is tne integrated fast portion of the TOF signal. Tne angular aistrioution was fit to the equation:

$$I(\theta) = 1 + 2bP_2(\cos \theta - \theta_0) \qquad (6)$$

by a least squares method. $b \approx -0.3 \pm 0.1$ and $\theta_0 = 14 \pm 5°$ gave the best fit. To nominally transform from tne laboratory to the center of mass frame of the molecule[21] a $\theta_0 = 8°$ was expected as calculated from the molecular beam velocity ano the average speed of the methyl radical. This agrees roughly with the measured shift of $14 \pm 5°$ in this distribution.

DISCUSSION

A. The Nature of the Excited State of Nitromethane

A simple molecular orbital picture for the π electron structure of the nitro group in nitromethane was given by Nagakura.[2] The orbitals and their symmetries (assuming C_{2v} for the nitro group) are:

$$b_2: \quad \phi_0 \quad = \quad 0.7133 \, N + 0.7009 \, (O_1 + O_2)/\sqrt{2} \tag{7}$$

$$a_2: \quad \phi_1 \quad = \quad (O_1 - O_2)/\sqrt{2} \tag{8}$$

$$b_1: \quad \phi_2 \quad = \quad 0.7009 \, N - 0.7133 \, (O_1 + O_2)/\sqrt{2} \tag{9}$$

The $2p\pi$ atomic orbitals for the nitrogen and two oxygen atoms are designated by N, O_1 and O_2. In the ground state, the b_2 and a_2 orbitals are filled, and the symmetry is A_1. The transfer of an electron from a_2 to b_1 is believed to be responsible for the strong peak in the absorption spectrum, near which the ArF laser is exciting. This excited state configuration has B_2 symmetry and the transition is therefore polarized in the molecular plane perpendicular to the C-N bond. More refined calculations[22,23] agree with this assignment of the 198 nm transiton as $^1B_2 \leftarrow {}^1A_1$, though a controversial assignment of the transition to a $\pi^* \leftarrow \sigma$ ($^1B_1 \leftarrow {}^1A_1$) has been proposed by Rabelais.

Assuming the $\pi^* \leftarrow \pi$ assignment is correct, the electronic excitation is localized on the NO_2 group and the dissociation would not be expected to proceed as a direct dissociation from the excited electronic state. The $\pi^* \leftarrow \pi$ state must be predissociated by an electronic state repulsive in the C-N bond or by a lower bound electronic state above its dissociation limit.

The $^1A_1$ repulsive electronic state described briefly by Harris[23] could predissociate the $^1B_2$ state in C_s and would correlate to $^2B_2$ excited state NO_2 product. This would be consistent with the emission studies as will be discussed. The predissociation is expected to be fast as indicated by the lack of structure in the absorption spectrum. The lack of strong anisotropy in the angular distribution could result from a combination of many factors: rotation of the excited molecule through a non-negligible angle between the excitation and dissociation process, the excitation of out-of-plane or antisymmetric stretching modes of the NO_2 group, or participation of another electronic state in the absorption with a parallel transition moment.

This paper has presented two different measurements of the anisotropy parameter, b. In the experiment performed on an effusive molecular beam of nitromethane with a low photon flux, b = -0.3 ± 0.1 was measured consistent with the perpendicular assignment of the transition. In the experiment performed at high photon flux with a supersonic molecular beam, the c.m. angular distribution was determined to be nearly isotropic, b = 0 ~ -0.1. Assuming no experimental error and admitting the uncertain statistics of the first measurement, what differences between the two experiments could have caused the discrepancy? An accepted difference between supersonic and effusive molecular experiments is that the rotation of the parent molecule in an effusive expansion is not relaxed, while it is to some degree in a supersonic expansion, so the rotation of the parent molecule after excitation but before dissociation will smooth the angular distribution of photofragments more in an effusive experiment. Here, however, the

supersonic expansion gives the more smoothed angular distribution, so this cannot explain the difference between the two measurements. A possible explanation for the differing measurements may result from the difference in photon flux in the two experiments assuming that the internal rotation of the nitromethane molecule has relaxed in the supersonic expansion. Ling and Wilson[24] have shown that for linear molecules, saturation of the parallel or perpendicular transitions by high photon fluxes causes a smearing of the measured angular distribution of photofragments. They point out that the effect is particularly small for perpendicular transitions as here the dipole moment vector is anywhere in a plane perpendicular to the dissociating bond. In the case of nitromethane, however, if the internal rotation of the NO_2 with respect to the CH_3 group is relaxed, the dipole moment vector which is perpendicular to the NO_2 plane is no longer defined by the entire plane perpendicular to the C-N bond. The overall rotation of the CH_3NO_2 molecule will not bring the dipole moment vector, $\vec{\mu}$, in perfect alignment with the electric field vector, $\vec{E}$, for a significant fraction of the molecules, yet these molecules will be dissociated with near unit probability at very high values of photon flux along with those molecules whose $\vec{\mu}$ becomes parallel with $\vec{E}$ during the molecules' rotation. The result is a more isotropic angular distribution of photofragments. This explanation may partially account for the more isotropic angular distribution measured on the supersonic molecular beam experiment at the high photon flux.

B.   Dynamics of the Dissociation

Conservation of energy allows us to write an expression for the partitioning of energy.

$$E_{avail} = h\nu + E_{int}^{P} - D_0(R - NO_2) = E_E + E_T + E_V + E_R \tag{10}$$

where the available energy, E_{avail}, consists of the photon energy, $h\nu$, plus the internal energy of the parent molecule, E_{int}^{P}, minus the energy, $D_0(R-NO_2)$, required to break the C-N bond. This energy is partitioned into the translational, rotational, vibrational, and electronic degrees of freedom of the fragments. An upper limit for the vibrational energy of the parent molecule would assume no relaxation of the vibrational modes in the supersonic expansion and may be calculated from the known vibrational frequencies[25] of nitromethane for the 240°C nozzle temperature; this gives 2.1 kcal/mole vibrational energy. As rotational relaxation is believed to follow translational relaxation and the velocity distribution of the nitromethane indicates translation has relaxed to <30°K, we will assume no significant contribution to the available energy from the overall rotations of the molecule or the one near free rotation about the C-N bond. As the translational energy distribution has been measured, the combined vibrational, rotational, and electronic energy of the fragments can be inferred. These two studies, in addition, have given information on the electronic energy of the products and the partitioning of internal energy between the CH_3 and NO_2 fragments, as will be discussed below.

i.   Fluorescence Emission Studies

Let us first consider the electronic state of the excited state NO_2 product. The spectroscopy and theory of NO_2 is reviewed in the first chapter of the spectral atlas of Hsu et al.[26] The ground state is designated as $X^2 A_1$ and the three lowest excited states are A $^2B_2$, B $^2B_1$ and C $^2A_2$. The nearness of these states causes mixing of the vibrational levels by vibronic coupling, Jahn- and Renner-Teller and spin-orbit interactions. As a result most of the spectrum of NO_2 has yet to be analyzed. Lifetime measurements have yielded a large number of different values depending on the excitation used.[27-30] When excited at 593.3 nm two lifetimes were observed which Stevens et al.[30] have attributed to the $^2B_2$ state (30 ± 5 µs) and the $^2B_1$ state (115 ± 10 µs). Our measurement of 35 ± 5 µs is not intended to be yet another value for the lifetime. All that can be said is that the lifetime falls within the range reported and that the excited NO_2 state that is formed is probably in the $^2B_2$ state. The fluorescence studies do not eliminate the possibility that some of the NO_2 product is formed in the ground state or the non-fluorescing $^2A_2$ state. If according to the majority of theoretical and experimental results (and consistent with our angular distribution) nitromethane is excited to the $^1B_2$ state at 193 nm, then the products $NO_2(A^2B_2)$ + CH_3 (X^2A_1'') have the same overall symmetry. It is also believed that the $^2B_2$ state of NO_2 is responsible for most of the visible emission.[31]

The emission spectrum has been studied by a number of workers. When NO_2 is directly excited by a single wavelength, a discrete structure is

observed superimposed on a broad continuum. Sakurai and Broida[32] measured the ratio of discrete to continuous emission as a function of excitation energy and found that the continuum emission increased with increasing energy. In a series of studies Kaufman et al.[28,33] explained the sharpness as due to emission from levels initially populated whereas the continuum is due in part to collisional relaxation to a large number of other radiating levels and in part to an inherent property of NO_2 in the absence of collisions. The lack of any discrete features in the emission spectra of Fig. 6 implies that the NO_2 is formed very high up in the vibrational manifold of the $^2B_2$ state where the spacing between levels is smaller. That the NO_2 is vibrationally hot is consistent with the low average translational energies found for the fragments.

II. Molecular Beam Studies

The analysis has shown that the primary process in the photodissociation of nitromethane at 193 nm is cleavage of the C-N bond to yield CH_3 and NO_2 radicals and that there are two distinct mechanisms for formation of these chemical products. The data further suggests that a significant (>10 percent) fraction of the NO_2 product formed in the dominant mechanism retains 72 kcal/mole of internal energy or more and dissociates to NO + O, as evidenced by the apparent loss of the slow NO_2 product depicted in Fig. 4. This interpretation is supported by the emission studies of the NO_2 product from the photodissociation of the series of nitroalkanes, which also indicate that much of the total available energy is retained as internal energy of the excited state NO_2. It is further supported by the observation of NO_2 fluorescence near the dissociation limit to NO + O.

The molecular beam study does not identify the electronic state of the products, but it is consistent with a large fraction of the NO_2 product being formed in the $^2B_2$ state. The total available energy for product translational + internal energy is 90 kcal/mole. As the largest amount of energy that goes into translational energy in the dissociation process is 44 kcal/mole, the major fraction of the NO_2 product contains much more internal energy than the electronic energy of the $^2B_2$ state, particularly considering the evidence that the alkyl group carries away little internal energy.

If one assigns the main feature of the product translational energy distribution shown in Fig. 4 to production of NO_2 in the excited $^2B_2$ state and subtracts the electronic energy, $E_E = 27.9$ kcal/mole[17,18], of the $^2B_2$ state from the total available energy, then the average fraction of the modified total available energy, $E_{avail}^* = E_{avail} - E_E$, that goes into translation is:

$$f_T = \frac{\overline{E_T}}{E_{avail}^*} = \frac{(13.4 + 16.2)}{2(90-27.9)} = 0.24 \pm 0.02 \qquad (11)$$

The major uncertainty in f_T is in the approximation of $\overline{E_T}$ for the major primary process. It is certainly lower than 16.2 kcal/mole, the $\overline{E_T}$ for the $NO_2(^2B_2)$ product distribution, because the slow $NO_2(^2B_2)$ product has undergone unimolecular decomposition, and it is larger than 13.4 $\overline{E_T}$ for the CH_3^+ distribution, as here the low translational energies from the 2 kcal/mole mechanism are included, so the true $\overline{E_T}$ for process (2) lies between these limits. Here we take the average and state the uncertainty due to these considerations. Thus, the average translational energy release, ~15 kcal/mole, is only 24 percent of the total available energy minus electronic energy, leaving a large fraction, 47 kcal/mole, for excitation of rotation and vibration of the CH_3 and NO_2 fragments.

Some characteristics of the excitation and dissociation suggest how this vibrational and rotational energy might be partitioned in the NO_2 and CH_3 fragments. First, if the symmetry of the ground state is preserved in the excited state, little rotational angular momentum will be generated during the separation of the fragments CH_3 and NO_2. Second, the change in geometry of the CH_3 group from near tetrahedral to near planar might be expected to excite the symmetric bend of the methyl radical, but only by 2-3 quanta if analogy is made with the recent experiments on the photodissociation of CH_3I.[34,35] Thus, most of the internal excitation will be found in the NO_2 fragment. The initial absorption of a photon by the NO_2 group might be expected to excite the bend and symmetric stretch of the NO_2 group in the $^1B_2$ state as this would be the case for π electron excitation in free NO_2. The geometry of the X $^1A_1$ state of nitromethane is given by Cox and Waring[36] as <NCH = 107.2°, <ONO = 125.3° and N-O = 1.224 Å; the $^1B_2$ excited state geometry has not been calculated

to our knowledge. The bond angles and lengths for ground $^2A_1$ NO_2 are 134° and 1.20 Å as compared to the theoretical values of 102° and 1.26 Å for the $^2B_2$ state.[37]

Though much information on the dominant dissociation mechanism of nitromethane has been derived from these experiments, only a few facts have been learned about the minor pathway. A possible explanation for a translational energy distribution that peaks sharply at such low energies might be internal conversion and dissociation from the ground electronic state of nitromethane to ground state products. This channel would be expected to release a much smaller fraction of the total available energy to translation than the dominant process of predissociation of the $\pi \rightarrow \pi^*$ state, presumably by a surface that is repulsive in the C–N bond correlating to excited state NO_2. If this ground state NO_2 product absorbed a 193 nm photon, it could be brought to the upper $^2B_2$ state of NO_2 which is thought to correlate to NO + O(^{1}D) at 117 kcal/mole.[38] This is consistent with the angular distribution of fast NO and O photofragments which resulted from a parallel transition, and with the maximum transla-tional energy release for the secondary dissociation being less than the total available energy of ~119 kcal/mole [148(hν) + 148(hν) –60(C–N) –117(ON–O(^{1}D))]. This explanation is not completely satisfactory for two reasons. First, dissociation from the ground state might be expected to have a translational energy distribution peaking at zero kcal/mole if there were no barrier to dissociation. Second, it is not clear to us why the proposed ground state product for the minor channel would differ in its cross section for absorption of a 193 nm photon from the $^2B_2$ NO_2

product from the major channel because these two electronic states are so strongly mixed at high internal energies. This dynamically distinct mechanism for producing CH_3 and NO_2 radicals requires further investigation.

ACKNOWLEDGMENT

REFERENCES

1. W. D. Taylor, T. D. Allston, M. J. Moscato, G. B. Fazekas, R. Kozlowski and G. A. Takas, Int. J. Chem. Kinet. 12, 231 (1980).

2. S. Nagakura, Mol. Phys. 3, 152 (1960).

3. J. W. Rabelais, J. Chem. Phys. 57, 960 (1972).

4. T. Fujikawa, T. Ohta and H. Kuroda, Chem. Phys. Lett. 28, 433 (1974).

5. W. M. Flicker, O. A. Musher, and A. Kupperman, J. Chem. Phys. 72, 2788 (1980).

6. P. E. Schoen, M. J. Marrone, J. M. Schnur and L. S. Golaber, NRL Memor. Report 4755, p.3 (1981); Chem. Phys. Lett. 90, 72 (1982).

7. K. Honda, H. Mikuni, and M. Takahasi, Bull. Chem. Soc. Japan 45, 3534 (1978).

8. I. M. Napier and R. G. W. Norrish, Proc. Roy. Soc. A 299, 317 (1967).

9. K. G. Spears and S. P. Brugge, Chem. Phys. Lett. 54, 373 (1978).

10. H. S. Kwok, G. Z. He, R. K. Sparks, and Y. T. Lee, Int. J. Chem. Kinet. 3, 1125 (1981).

11. Y. T. Lee, J. D. McDonald, P. R. LeBreton and D. R. Herschbach, Rev. Sci. Instrum. 40, 1402 (1969).

12. See, for example, Aa. S. Sudbo, P. A. Schulz, Y. R. Shen, and Y. T. Lee, J. Chem. Phys. 69, 2312 (1978).

13. This background is presumably due to scattered light from the intense laser dissociating or desorbing diffusion pump oil from the wall behind the interaction region in the viewing region of the detector. As would be expected there, it appears at a typical hydrocarbon fragment mass.

14. M. Kawasaki, S. J. Lee and R. Bersohn, J. Chem. Phys. $\underline{40}$, 64 (1964).

15. A. Fontijn, C. B. Meyer, and H. I. Schiff, J. Chem. Phys. $\underline{40}$, 64 (1964).

16. G. Inove, Y. Nakata, Y. Usui, H. Akimoto, and M. Okuda, J. Chem. Phys. $\underline{70}$, 3689 (1979).

17. G. D. Gillespie and A. U. Khan, J. Chem. Phys. $\underline{65}$, 1624 (1976).

18. J. C. D. Brand, K. J. Cross, and A. R. Hoy, Can. J. Phys. $\underline{60}$, 1081 1982).

19. This assumes that the cracking pattern of NO_2 is essentially the same for the range of internal energies of the NO_2 product.

20. Because the main feature here is due to the remaining NO_2 product, this is only strictly true if the fraction of NO_2 that absorbs another photon is small. If the fraction were larger, then the relative power dependence would be expected to be even stronger than linear.

21. G. E. Busch and K. R. Wilson, J. Chem. Phys. $\underline{56}$, 3638 (1972).

22. K. L. McEwen, J. Chem. Phys. $\underline{32}$, 1801 (1960).

23. L. E. Harris, J. Chem. Phys. $\underline{58}$, 5615 (1973).

24. J. H. Ling and K. R. Wilson, J. Chem. Phys. $\underline{65}$, 3 (1976).

25. G. Geisler and H. Kessler, Ber. Bunsen Physik. Chem. $\underline{68}$, 571 (1964).

26. D. K. Hsu, D. L Monts, and R. N. Zare, Spectral Atlas of Nitrogen Dioxide 5530 to 6480A, Academic Press, N.Y. (1978).

27. D. Neuberger and A. B. F. Duncan, J. Chem. Phys. $\underline{22}$, 1693 (1954).

28. V. M. Donnelly and F. Kaufman, J. Chem. Phys. $\underline{66}$, 4100 (1977); ibid. $\underline{69}$, 1456 (1978).

29. S. E. Scnwartz and H. S. Johnston, J. Chem. Phys. 51, 1286 (1969).

30. C. G. Stevens, M. W. Swagel, R. Wallace, and R. N. Zare, Chem. Phys. Lett. 18, 456 (1973).

31. H. Okabe, Photochemistry of Small Molecules, Wiley-Interscience, N.Y. (1978) p. 232.

32. K. Sakurai and H. P. Broida, J. Chem. Pnys. 50, 2404 (1969).

33. D. G. Keil, V. M. Donnelly, and F. Kaufman, J. Chem. Phys. 73, 1514 (1980).

34. H. W. Hermann and S. R. Leone, J. Chem. Phys. 76, 4766 (1982).

35. R. K. Sparks, K. Shobatake, L. R. Carlson and Y. T. Lee, J. Chem. Phys. 75, 3838 (1981).

36. A. P. Cox and S. Waring, J. Chem. Soc., Faraday Trans. 2, 68, 1624 (1976).

37. G. D. Gillispie, A. U. Khan, R. P. Hosteng, and M. Krauss, J. Chem. Phys. 63, 3425 (1975).

38. R. J. S. Morrison, B. H. Rockney and E. R. Grant, J. Chem. Phys. 75, 2643 (1981).

39. R. E. Center and A. Mandl, J. Chem. Phys. 57, 4104 (1972).

40. T. M. Miller and B. Bederson, Adv. At. Mol. Phys. 13, 1 (1977).

41. D. Krajnovich, F. Huisken, Z. Znang, Y. R. Shen and Y. T. Lee, J. Chem. Phys. 77, 5977 (1982).

APPENDIX I: COMPARISON OF EXPERIMENTAL AND CALCULATED CH$_3$:NO$_2$ RATIOS

The true experimental CH$_3$:NO$_2$ ratio at laboratory angle Θ is related to the observed CH$_3^+$:NO$^+$ ion signal ratio according to

$$\frac{N_{CH_3}(\Theta)}{N_{NO_2}(\Theta)} = \frac{N_{CH_3^+}(\Theta)}{N_{NO^+}(\Theta)} \cdot \frac{\sigma_{ion}(NO_2)}{\sigma_{ion}(CH_3)} \cdot \frac{f(NO^+|NO_2)}{f(CH_3^+|CH_3)} ,$$

where $\sigma_{ion}(NO_2)$ is the ionization cross section of NO_2, $f(NO^+|NO_2)$ is the fraction of those NO_2 radicals which are ionized which give NO^+, and similarly for $\sigma_{ion}(CH_3)$ and $f(CH_3^+|CH_3)$. At $\Theta = 40°$, the observed CH$_3^+$ and NO$^+$ signal levels were 0.30 and 0.98 counts/pulse, respectively. (We will ignore the contribution of NO radicals from secondary NO_2 photodissociation to the NO$^+$ signal, since this contribution (~20 percent) is small compared to errors involved in the determination of the radical fragmentation patterns, as will be discussed below.)

The ionization cross sections were estimated using the following empirical correlation between peak ionization cross section and the polarizability[39]

$$\sigma_{ion} = 36\sqrt{\alpha} - 18,$$

where σ_{ion} and α are in units of $Å^2$ and $Å^3$, respectively. Molecular polarizabilities were approximated as the sum of the atomic polarizabilities. This is expected to be a good approximation except in the case of highly polarizable one-electron atoms such as H or the alkalis) where the atomic polarizability tends to overestimate the contribution to the molecular polarizability. This is illustrated by the fact that the polarizabilities

of atomic and molecular hydrogen are nearly equal. Therefore, for H, we took $\alpha_H = (1/2)\alpha_{H_2} = 0.3$. The values of the other atomic polarizabilities were taken from Ref. 40: $\alpha_C = 1.8$, $\alpha_N = 1.1$, $\alpha_O = 0.8$. Thus, $\sigma_{ion}(CH_3) = 41$, $\sigma_{ion}(NO_2) = 41$. (If α_H is used instead of $(1/2)\alpha_{H_2}$ to calculate the contribution of H to the CH_3 polarizability, $\sigma_{ion}(CH_3)$ increases to 50. This difference is negligible at the present level of comparison.)

Methyl radicals fragment mainly to give CH_3^+, CH_2^+ and CH^+ in the ionizer. We measured the following signal ratio in our experiment:

$$m/e = 15:14:13 = 100:167:43.$$

The $m/e = 15$ and 13 TOF distributions look identical. Therefore all of the $m/e = 13$ signal is due to CH^+. However, the TOF distribution at $m/e = 14$ clearly shows contributions from both CH_3 (as CH_2^+) and NO_2 (as N^+). Unfortunately the data quality at $m/e = 14$ is quite poor, due to high detector background at this mass. We estimate roughly that only 1/3 of the $m/e = 14$ signal is due to CH_3. (This is the weakest point in this analysis.) Then, $CH_3^+:CH_2^+:CH^+ = 100:56:43$, and $f(CH_3^+|CH_3) = 0.50$.

NO_2 radicals fragment mainly to NO^+, O^+ and N^+. (The NO_2^+ signal is 10-20 times lower than the NO^+ signal and may be safely ignored.) We measured

$$CH_3^+:NO^+:O^+ = 15:100:29.$$

Using this data, together with the assumption that 2/3 of the m/e = 14 signal is due to NO_2, we obtain the following NO_2 fragmentation pattern:

$$NO^+:O^+:N^+ = 100:29:16.$$

This gives $f(NO^+|NO_2) = 0.69$.

The experimental $CH_3:NO_2$ ratio at 40° is therefore

$$\frac{N_{CH_3}(40°)}{N_{NO_2}(40°)} = \frac{0.30}{0.98} \times \frac{41}{41} \times \frac{0.69}{0.50} = 0.42.$$

If, at the other extreme, all of the m/e = 14 signal is ascribed to CH_2^+, we get $f(CH_3^+|CH_3) = 0.32$, $f(NO^+|NO_2) = 0.78$, and

$$\frac{N_{CH_3}(40°)}{N_{NO_2}(40°)} = 0.75.$$

The theoretical $CH_3:NO_2$ ratio at any angle is automatically calculated by the c.m. → LAB transformation program using the CH_3 and NO_2 P(E')'s for CH_3 and NO_2, respectively. The two P(E')'s must be normalized as shown in Fig. 4 (to properly take into account the loss of slow NO_2). The details of the general calculation are reviewed in Appendix B of Ref. 41. The result is

$$\frac{N_{CH_3}(40°)}{N_{NO_2}(40°)} = 0.63.$$

The experimental and calculated $CH_3:NO_2$ ratios agree reasonably well. (If anything, the experimental $CH_3:NO_2$ ratio is too small, indicating "too much" NO_2 relative to CH_3.) Therefore, we cannot assume that a large fraction of the total NO_2 primary product undergoes secondary photodissociation. This result forms the basis for the assumption that it must be the slow NO_2 formed in the minor primary photodissociation process [which gives rise to the blip in the CH_3 P(E')] which is responsible for the strongly saturated secondary photodissociation signal.

APPENDIX II: CALCULATION OF FITS TO NO^+ AND O^+ DATA.

Tne contribution of NO_2 to the NO^+ ana O^+ data is calculateo using tne NO_2 P(E') shown in dashed line in Fig. 4 ano the nitromethane beam velocity distribution for the distribution of c.m. velocities. We want to fit the shoulders in the NO^+ and O^+ TOF distributions by aojusting the P(E') and anisotropy parameter for the secondary photodissociation reaction:

$$NO_2 \rightarrow NO + O, \qquad\qquad (5)$$

and varying the contributions of NO and O relative to NO_2. Strictly speaking, when calculating the laboratory angular and TOF distributions of NO and O, we shoula use the laboratory number density angle-velocity distribution of the primary NO_2 product in place of the nitromethane beam velocity distribution to represent the distribution of c.m. velocities. Here we are assuming that only the slow NO_2 produceo via tne minor primary dissociation pathway undergoes seconoary photodissociation. This NO_2 is concentrated in a fairly narrow cone about the original nitromethane beam direction. Since much more translational energy is released in the secondary reaction (5) than in the minor primary dissociation reaction, the calculated NO and O angular and TOF aistributions are insensitive to the details of the energy release in the primary reaction. In tne fits to be presenteo below, we simply approximated tne parent NO_2 c.m. velocity distribution for reaction (5) by the nitromethane beam velocity. We will not justify tnis approximation in oetail here, but it is, in fact, a very good approximation in this case.

The relative contributions of NO_2 and NO to the NO^+ signal should be given by

$$N_{NO}^+(\Theta,t) = N_{NO_2}(\Theta,t) + \epsilon \cdot \frac{\sigma_{ion}(NO)}{\sigma_{ion}(NO_2)} \cdot \frac{f(NO^+|NO)}{f(NO^+|NO_2)} \cdot N_{NO}(\Theta,t),$$

where $N_{NO_2}(\Theta,t)$ is calculated from the NO_2 $P(E')$ in dashed line in Fig. 4, using an isotropic c.m. angular distribution, and $N_{NO}(\Theta,t)$ is calculated from a $P(E')$ and anisotropy parameter describing reaction (5). ϵ is the ratio of the fraction of NO_2 which undergoes secondary photo-dissociation to the fraction of NO_2 which survives. (For other notation, see Appendix I.) Similarly, the relative contributions of NO_2, NO and O to the O^+ signal should be given by

$$N_O^+(\Theta,t) = N_{NO_2}(\Theta,t) + \frac{\epsilon}{\sigma_{ion}(NO_2) \cdot f(O^+|NO_2))} \cdot$$

$$[\sigma_{ion}(NO) \cdot f(O^+|NO) \cdot N_{NO}(\Theta,t) + \sigma_{ion}(O) \cdot N_O(\Theta,t)].$$

We began by adjusting the $P(E')$ for reaction (5) to fit the shape of the shoulder in the NO^+ TOF at 40° (assuming b = 0). We obtained a good fit with the $P(E')$ shown in Fig. 14, which has a mean translational energy of 31 kcal/mole. However, using this $P(E')$ and b = 0, the NO_2:NO ratio which gave a good fit to the magnitude of the shoulder at 40° did not give a good fit to the shoulder heights at smaller angles; the calculated shoulders were too small at 10° and 25°. To compensate for this, a positive anisotropy parameter for reaction (5) was required. The best-fits to the NO^+ TOF

data shown in Fig. 15 were calculated using the P(E') in Fig. 14, b = +0.5, and the following NO_2:NO ratio:

$$N_{NO^+}(\Theta,t) = N_{NO_2}(\Theta,t) + 0.3 \, N_{NO}(\Theta,t).$$

Therefore it appears that the secondary photodissociation of NO_2 occurs via a parallel transition. From the empirically determined NO_2:NO ratio we have:

$$\epsilon \cdot \frac{\sigma_{ion}(NO)}{\sigma_{ion}(NO_2)} \cdot \frac{f(NO^+|NO)}{f(NO^+|NO_2)} = 0.3,$$

or

$$\epsilon \cdot f(NO^+|NO) = 0.27.$$

The corresponding fit to the measured NO^+ laboratory angular distribution is shown in Fig. 16.

To consistently fit the O^+ TOF distribution, we must use the same P(E') and anisotropy parameter for reaction (5), and an NO_2:NO:O ratio which is constrained by

$$N_{O^+}(\Theta,t) = N_{NO_2}(\Theta,t) + 3.84 \, \epsilon \cdot f(O^+|NO) \cdot N_{NO}(\Theta,t)$$
$$+ 1.72 \, \epsilon \cdot N_O(\Theta,t),$$

where we have used the NO_2 fragmentation pattern and ionization cross sections specified in Appendix I.

Unfortunately, we had no way of determining the NO fragmentation pattern in this experiment. At first we assumed that $f(O^+|NO) = 1-f(NO^+|NO)$ (i.e., all NO is ionized to either NO^+ or O^+). However, using this assumption, we could not get a satisfactory fit to the O^+ shoulder for any value of ϵ (the NO contribution was always too large compared to the O contribution). Evidently, some of the NO also fragments to N^+ in the ionizer. By arbitrarily assuming that $f(O^+|NO) = 1/2[1-f(NO^+|NO)]$, we were able to obtain the fit to the O^+ data shown in Fig. 17, using the value $\epsilon = 0.50$. This ϵ value implies that 1/3 of the total NO_2 primary product (less that fraction which spontaneously decomposes) undergoes secondary photodissociation.

The area under the CH_3 $P(E')$ in Fig. 4 is 36 percent larger than the area under the NO_2 $P(E')$. If all of this 36 percent difference were due to NO_2 which undergoes secondary photodissociation there would be almost perfect agreement with the ϵ value deduced above. However, part of the 36 percent difference is undoubtedly due to spontaneous unimolecular decay of hot NO_2 ($^2B_2$) produced in the major primary dissociation process. Therefore, the value $\epsilon = 0.50$ is a bit on the high side. Still, given the guesswork involved in the above analysis, we do not feel that this discrepancy is fatal. (If, on the other hand, we had deduced a value of $\epsilon \geq 1$, we would have been compelled to abandon the hypothesis that the secondary photo-dissociation signal is due to NO_2 produced in the minor primary dissociation process.)

The spontaneous decay of hot NO_2 from the major primary dissociation process is also reflected in the NO^+ and O^+ TOF distributions at small angles. The hottest NO_2 is formed in low recoil energy events, and, in the laboratory, should appear near the molecular beam velocity. The flight time corresponding to the nominal c.m. (CH_3NO_2) is ~150 μsec. The actual NO^+ and O^+ TOF data is smeared out in the vicinity of the c.m. velocity, due to spontaneous decay of the hottest NO_2. The smearing, however, is not too severe, suggesting that even the hottest NO_2 radicals are not too far above the $NO(^2\Pi) + O(^3P)$ dissociation limit. (Recall that the maximum possible NO_2 excess energy is 18 kcal/mole.)

Table 1. Power dependence of the relative shoulder intensity in the NO$^+$
          TOF spectrum at $\Theta = 40°$.

Pulse Energy (mJ)	Photon Flux[+] (photons/cm^2-pulse)	Laser Intensity[+] (MW/cm^2)	$\frac{S(15-35)}{S(36-120)} \pm \sigma$
0.7*	1.7×10^{16}	1.3	0.045 ± 0.008
2.0	4.9×10^{16}	3.6	0.049 ± 0.005
3.3*	8.0×10^{16}	5.9	0.047 ± 0.005
20	4.9×10^{17}	36	0.062 ± 0.003
33*	8.0×10^{17}	59	0.067 ± 0.003

*These measurements correspond to the data shown in Fig. 12.
[+]Calculated assuming a 4 mm^2 laser spot size at the molecular beam and a
14 ns laser pulse duration.

FIGURE CAPTIONS

Fig. 1.   Some energetically allowed dissociation channels of CH_3NO_2
excited at 193 nm. ΔH^0_{300} values were calculated from
ΔH^0_{f300} values tabulated in S.W. Benson, <u>Thermochemical</u>
<u>Kinetics</u>, 2nd ed. (John Wiley and Sons, New York, 1976), or
estimated using Benson's rules. Only ground electronic state
products are shown; NO may be produced in either spin orbit state
and NO_2 may be formed in the X^2A_1, A^2B_2, B^2B_1, or
C^2A_2 states.

Fig. 2.   TOF distributions of m/e = 15, CH_3^+, at three angles to the
molecular beam. ● Experimental points, ——— best fit
calculated using the solid-line P(E') in Fig. 4 and b = 0.

Fig. 3.   Laboratory angular distribution of the CH_3^+ signal. ● Experi-
mental points. Error bars represent plus or minus one standard
deviation of the statistical counting error; ——— calculated
using the solid-line P(E') in Fig. 4 and b = 0.

Fig. 4.   Center-of-mass translational energy distributions for the products
of the primary photodissociation reaction $CH_3NO_2 \rightarrow CH_3^+$ +
NO_2. ——— Derived from CH_3^+ angular and TOF
distributions; – – – – derived from NO_2^+ TOF distributions.
The uncertainty in fitting the feature at ~100 µsec in the
CH_3^+ TOF distributions (Fig. 2) is represented by the shaded
area near 2 kcal/mole in the solid-line P(E'). The top border of
the grey area fits the 10° TOF perfectly; the lower border fits
the 40° TOF well.

Fig. 5.   Fluorescence decay of NO_2^* from the photolysis of nitromethane.

Fig. 6.   Dispersed fluorescence due to electronically excited NO_2 from
the photolysis of nitrometnane at 193 nm. The dissocition limit
shown is for $NO_2 \rightarrow NO + O(^3P)$.

Fig. 7.   Dispersed fluorescence of NO_2^* formed by the photodissociation
of R-NO_2. The spectra are unchanged for the four different R
groups ($(CH_3)_3CNO_2$ is not shown).

Fig. 8.   Dispersed fluorescence from the photolysis of nitromethane by a
focused 193 nm laser.

Fig. 9.   TOF distributions of m/e = 46, NO_2^+, at three angles to the
molecular beam. ● Experimental points; ——— best fit calcu-
lated using the dashed-line P(E') in Fig. 4, assuming b = 0.

Fig. 10.   TOF distributions of m/e = 30, NO^+, measured at three angles to
the molecular beam. Fits are shown in Appendix II, Fig. 15.

Fig. 11.   TOF distribution of m/e = 16, O^+, measured at 10° from the
molecular beam. Fits are snown in Appendix II, Fig. 17.

Fig. 12. NO^+ TOF distributions measured at tnree laser pulse energies.
All tnree distributions were measured at $\Theta = 40°$ and have been
normalized to the same peak height.

Fig. 13.   Angular distribution of the methyl radicals formed by the photo-
dissociation of nitromethane at 193 nm in the effusive molecular
beam apparatus. The solid curve is tne best fit to the equation
$I(\theta) = A[1 + 2bP_2(\cos(\theta-\theta_0))]$ using b = -0.30 and $\theta_0 = 14°$.

Fig. 14.   Approximate rorm of the center-of-mass product translational
energy distribution for the secondary photodissociation reaction
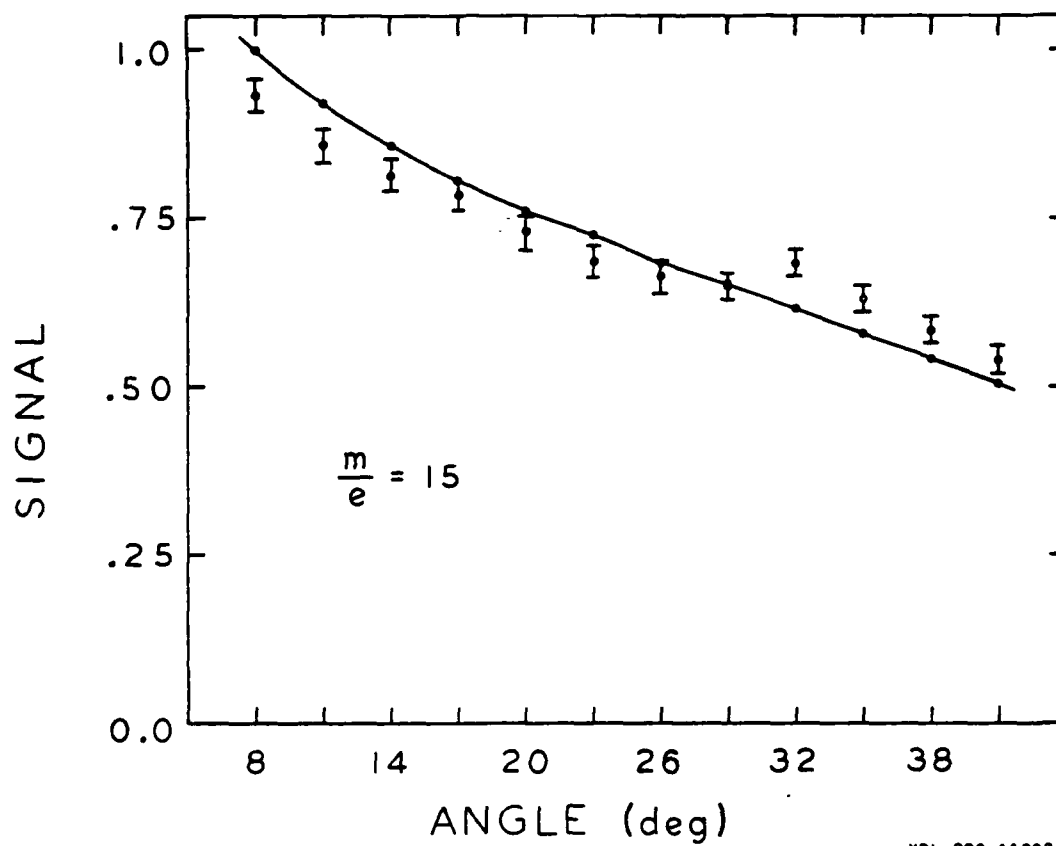$NO_2 \rightarrow NO + O$.

Fig. 15. TOF distributions of NO^+. ● Experimental points (same as
Fig. 10); ————— best fit, obtained by adding the individual
contribution of NO_2 (——— – ———) and NO (– – –) to the NO^+
signal. The NO_2 contribution was calculated using the
dashed-line $P(E')$ in Fig. 4 and b = 0. The NO contribution was
calculated using the $P(E')$ in Fig. 14 and b = +0.5. Spontaneous
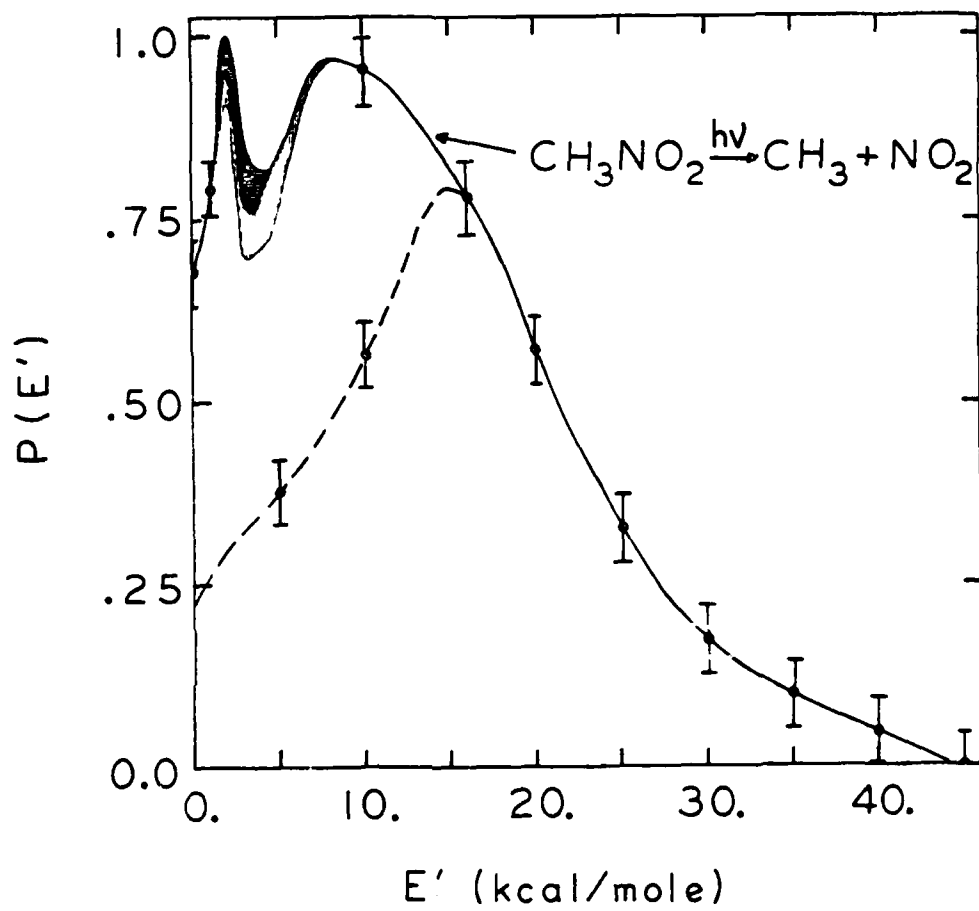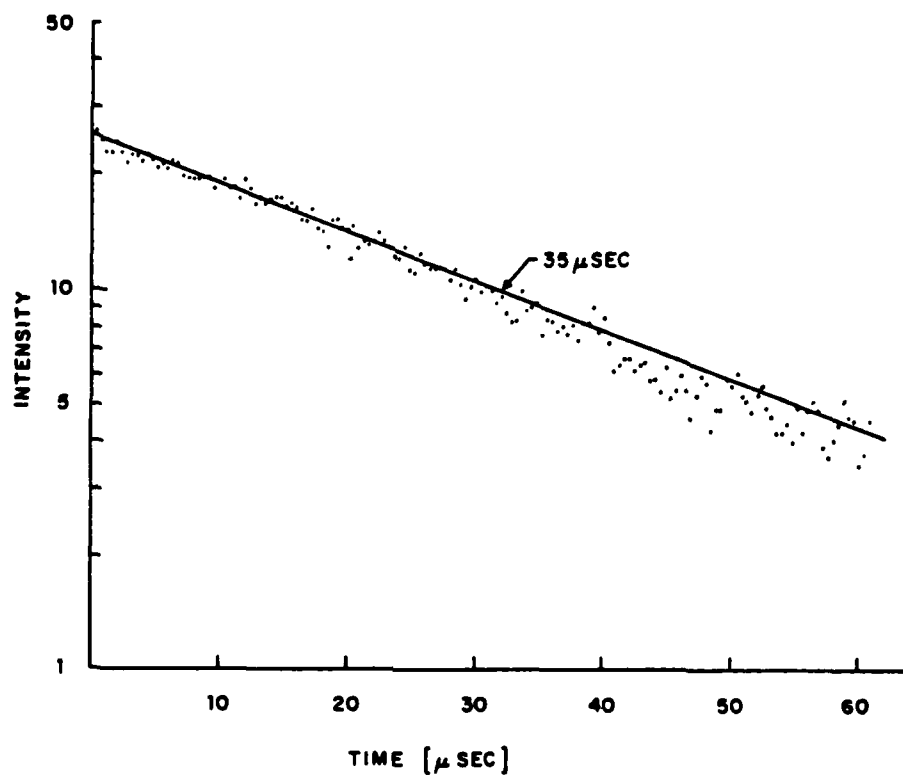unimolecular decay of hot NO_2 was neglected.

Fig. 16. Laboratory angular distribution of the NO^+ mass spectrometer
signal. ● Experimental points; ————— fit obtained by adding
the individual contributions of NO_2 and NO shown in dashed
lines. The relative contributions of NO_2 and NO to the total
was kept the same as for the fits of the TOF distributions of
NO^+ (Fig. 15). (For the experimental points, $\pm 2\sigma$ error bars are
roughly the size of the dots shown.)

Fig. 17. TOF distributions of O^+. ● Experimental points (same as Fig.
11); ————— best fit, obtained by adding the individual
contributions of NO_2 (——— – ———), NO (– – – –) and
O (——— . ———) to the O^+ signal. The NO_2 contribution was
calculated using the dashed-line $P(E')$ in Fig. 4 and b = 0. The
NO and O contributions were calculated using the $P(E')$ in Fig. 14
and b = +0.5. Spontaneous unimolecular decay of hot NO_2 was
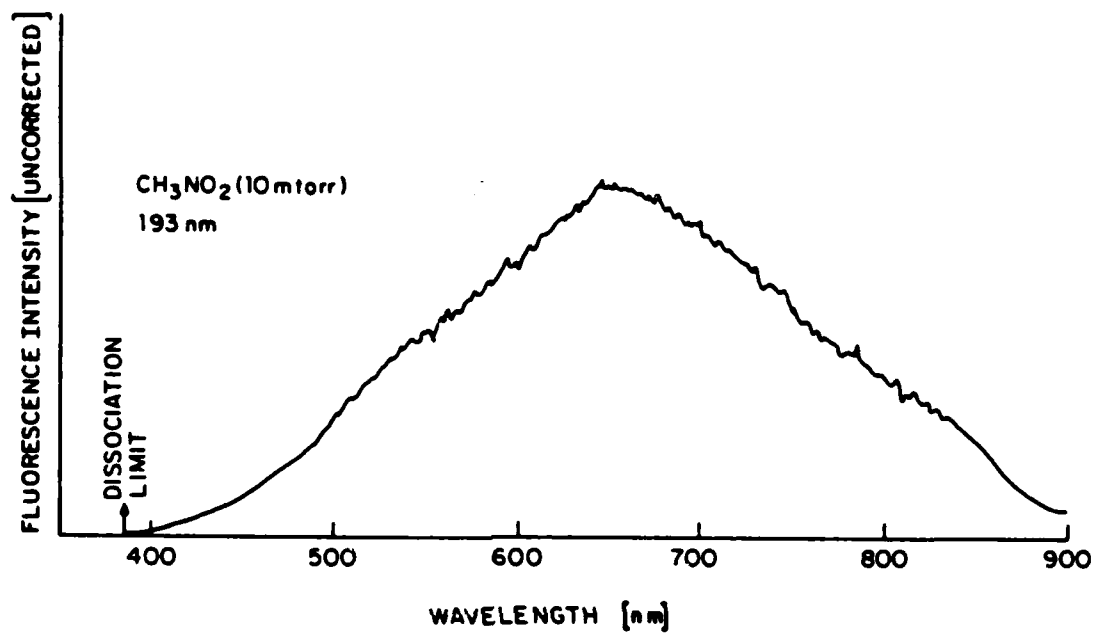neglected.

XBL 832-8223

NUMBER DENSITY vs FLIGHT TIME (μsec)

$\frac{m}{e} = 15$ 10°

25°

40°
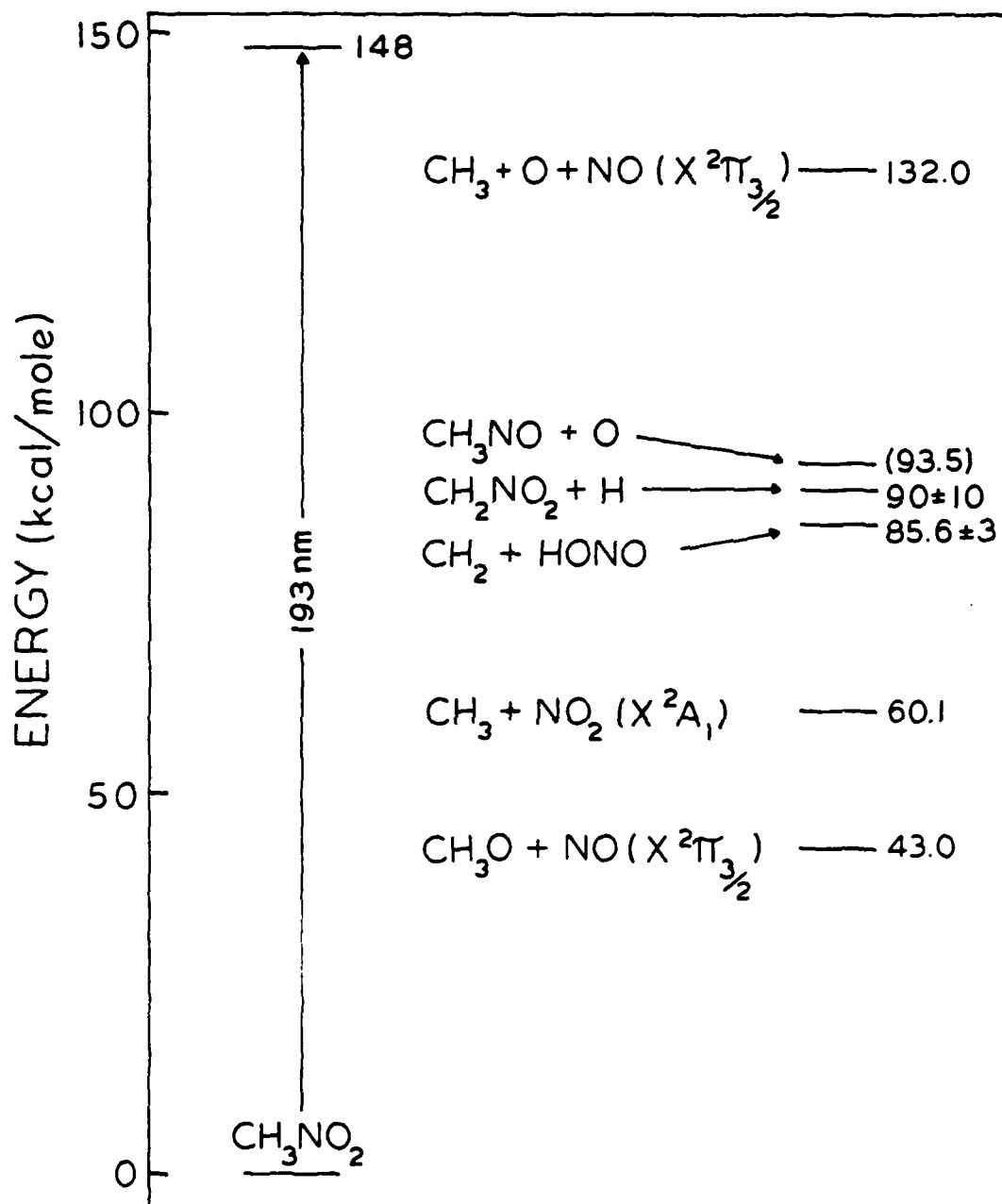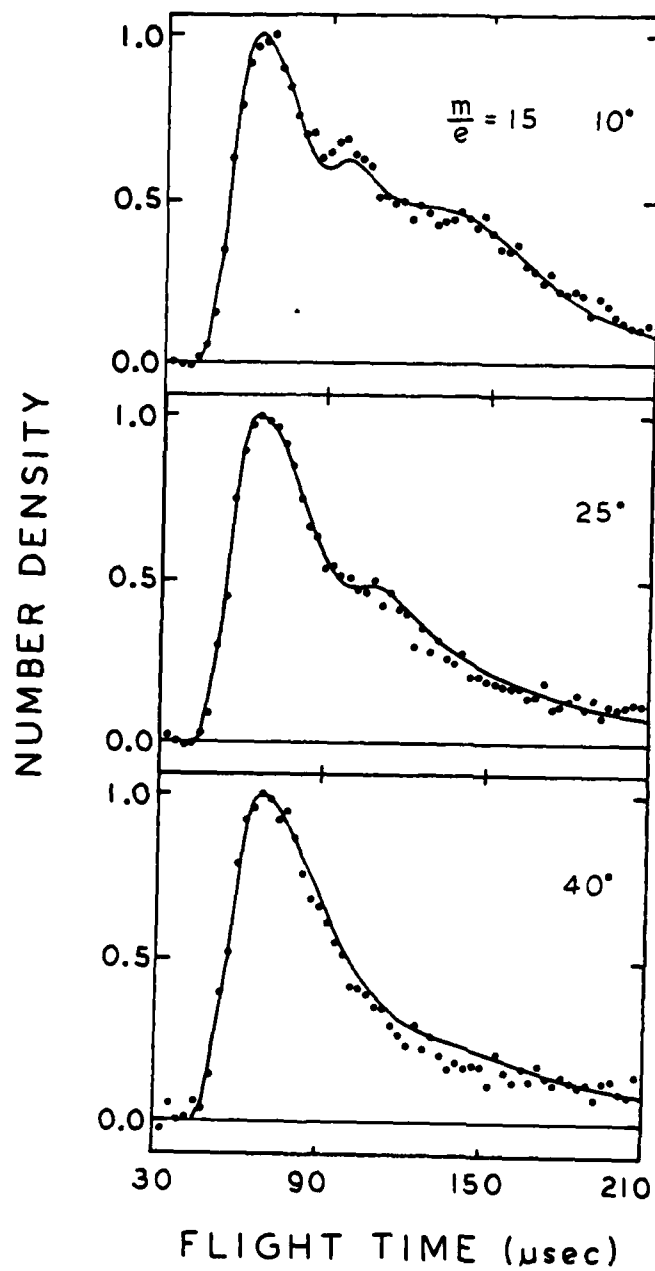
XBL 809-11843

XBL 829-11839

$$CH_3NO_2 \xrightarrow{h\nu} CH_3 + NO_2$$

XBL 829-11840

XBL 832-8190

CH₃NO₂ (10 mtorr)
193 nm

FLUORESCENCE INTENSITY [UNCORRECTED]

DISSOCIATION LIMIT

WAVELENGTH [nm]

XBL 832-8189

FLUORESCENCE INTENSITY [UNCORRECTED]

CH_3NO_2 (2 mtorr)
193 nm (FOCUSED)

NO_2 ($^2B_2 - {}^2A_1$)

CH ($^2\Delta - {}^2\Pi$)

CN ($^2\Sigma - {}^2\Sigma$)

WAVELENGTH [nm]

340 360 380 400 420 440 460 480 500 520 540

XBL 832-8188

FLIGHT TIME (μsec)
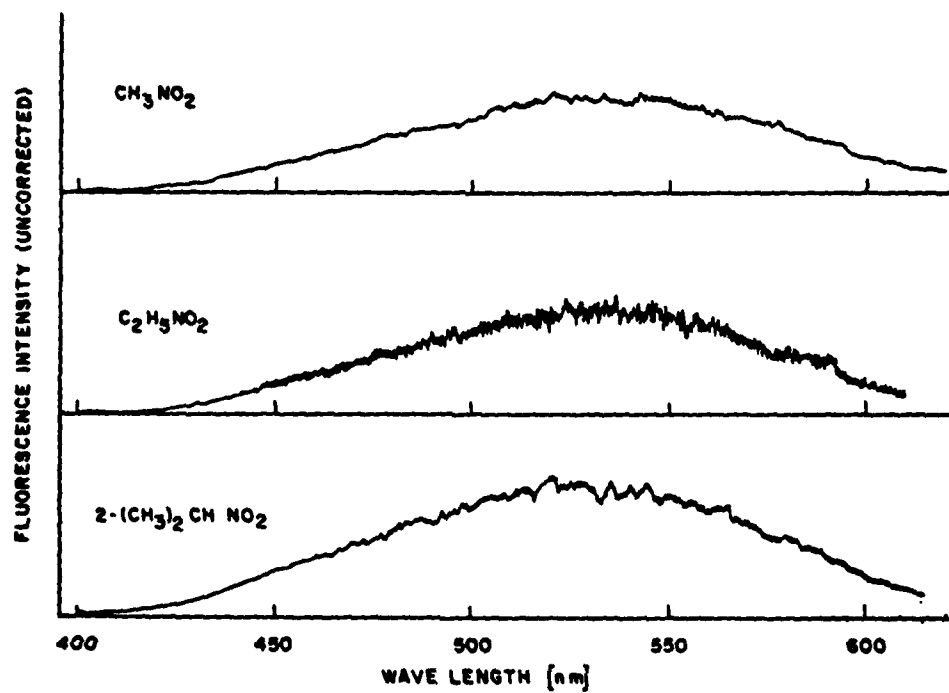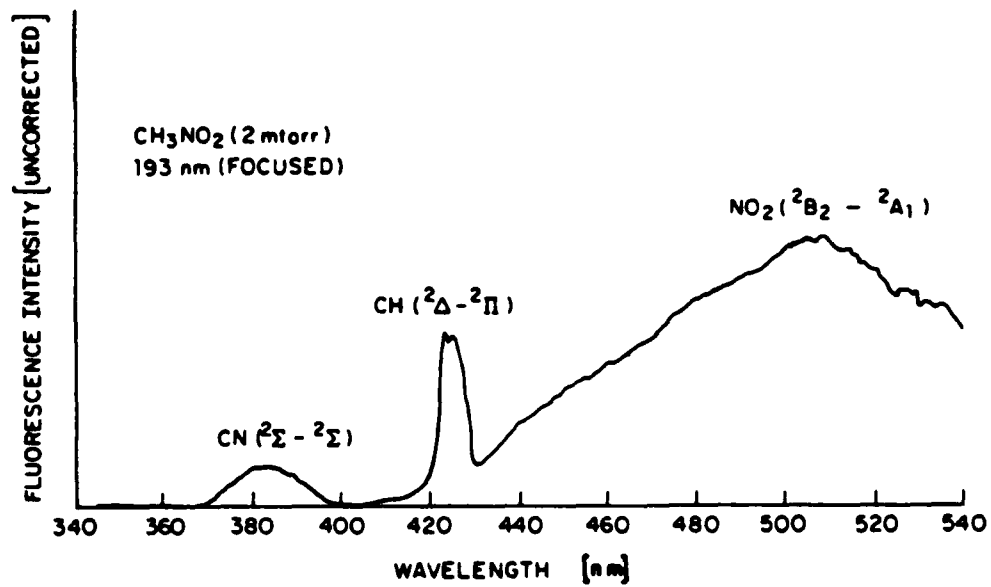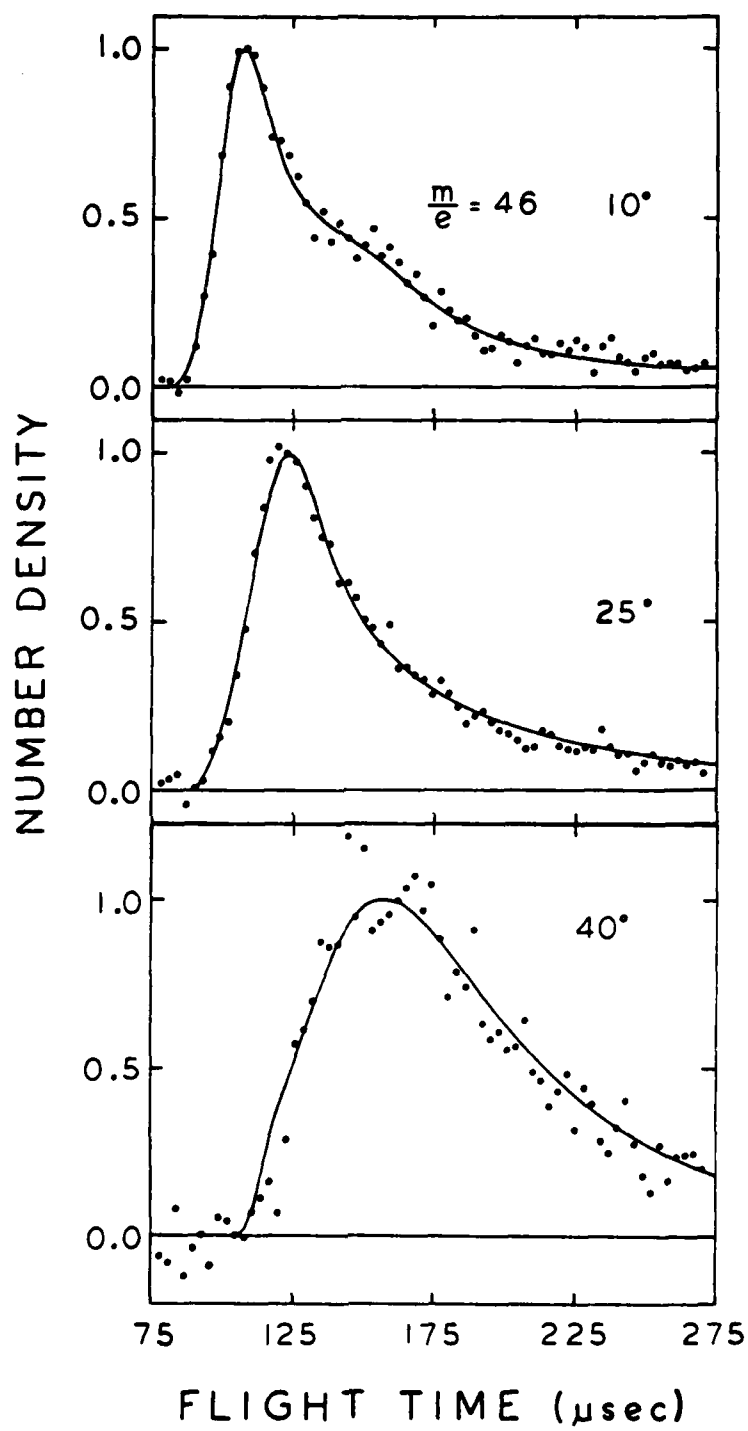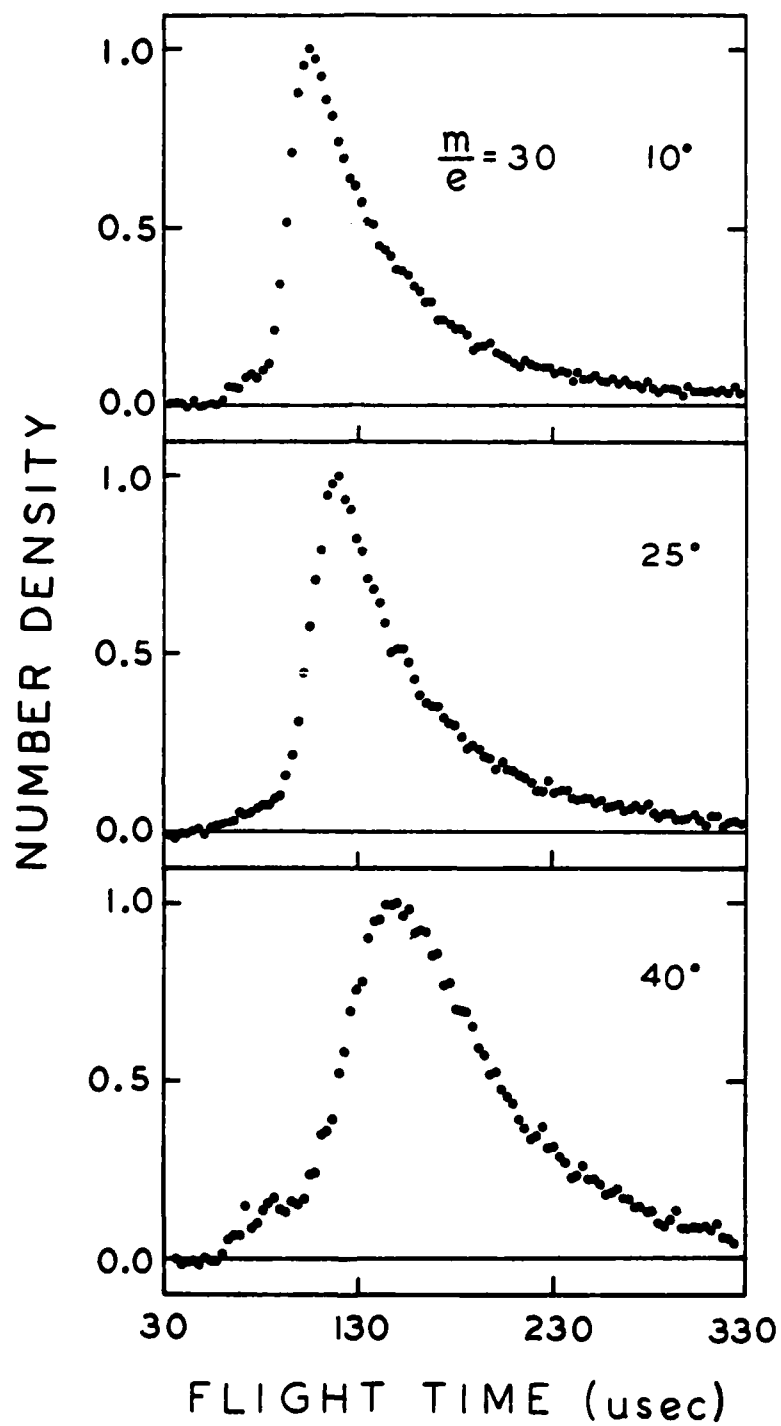
XBL 829-11842

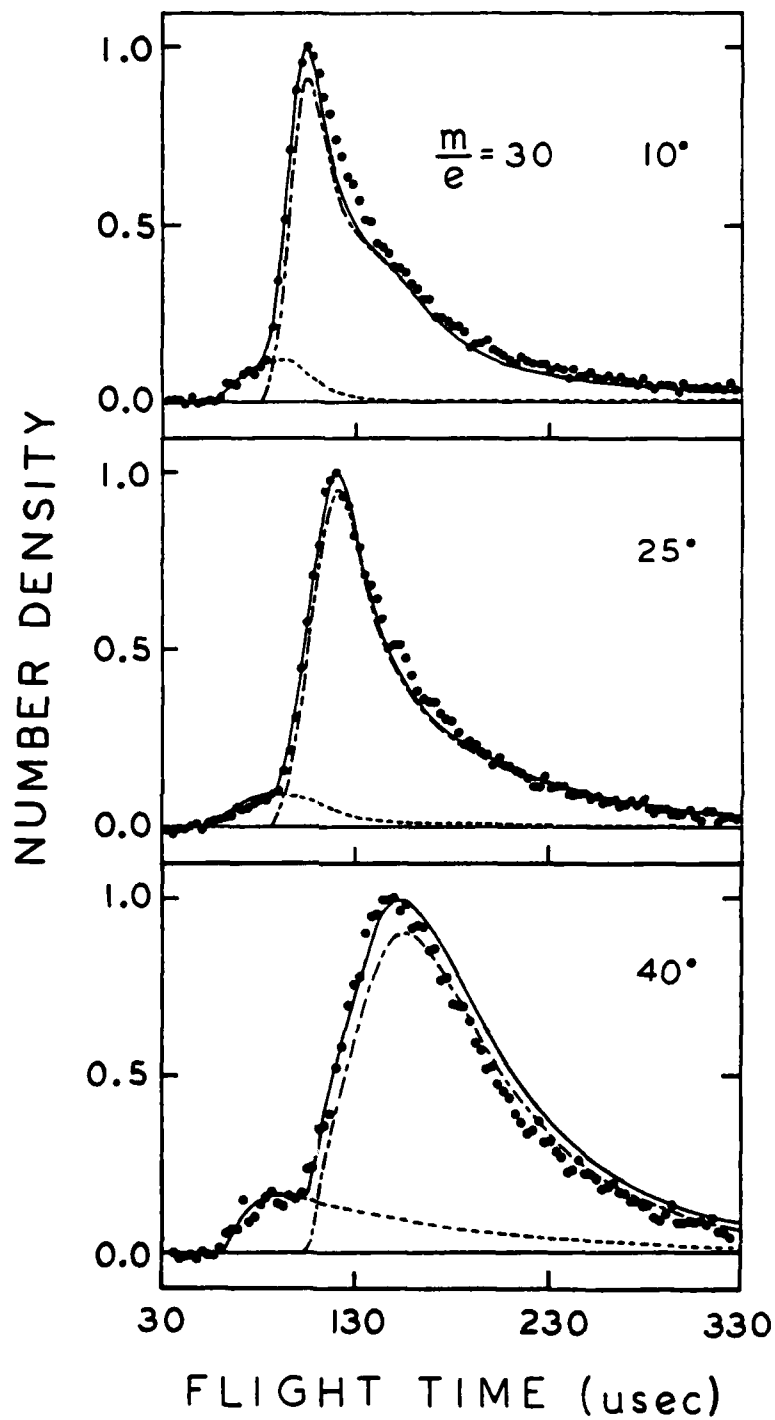XBL 829-11841
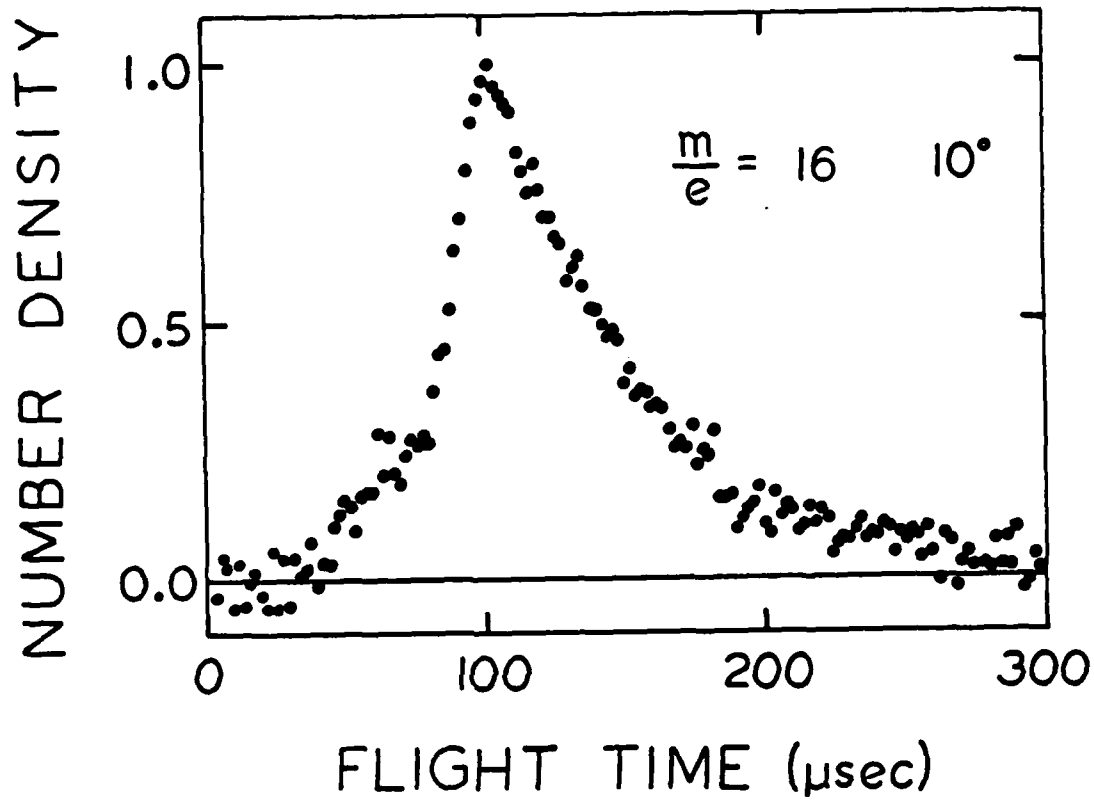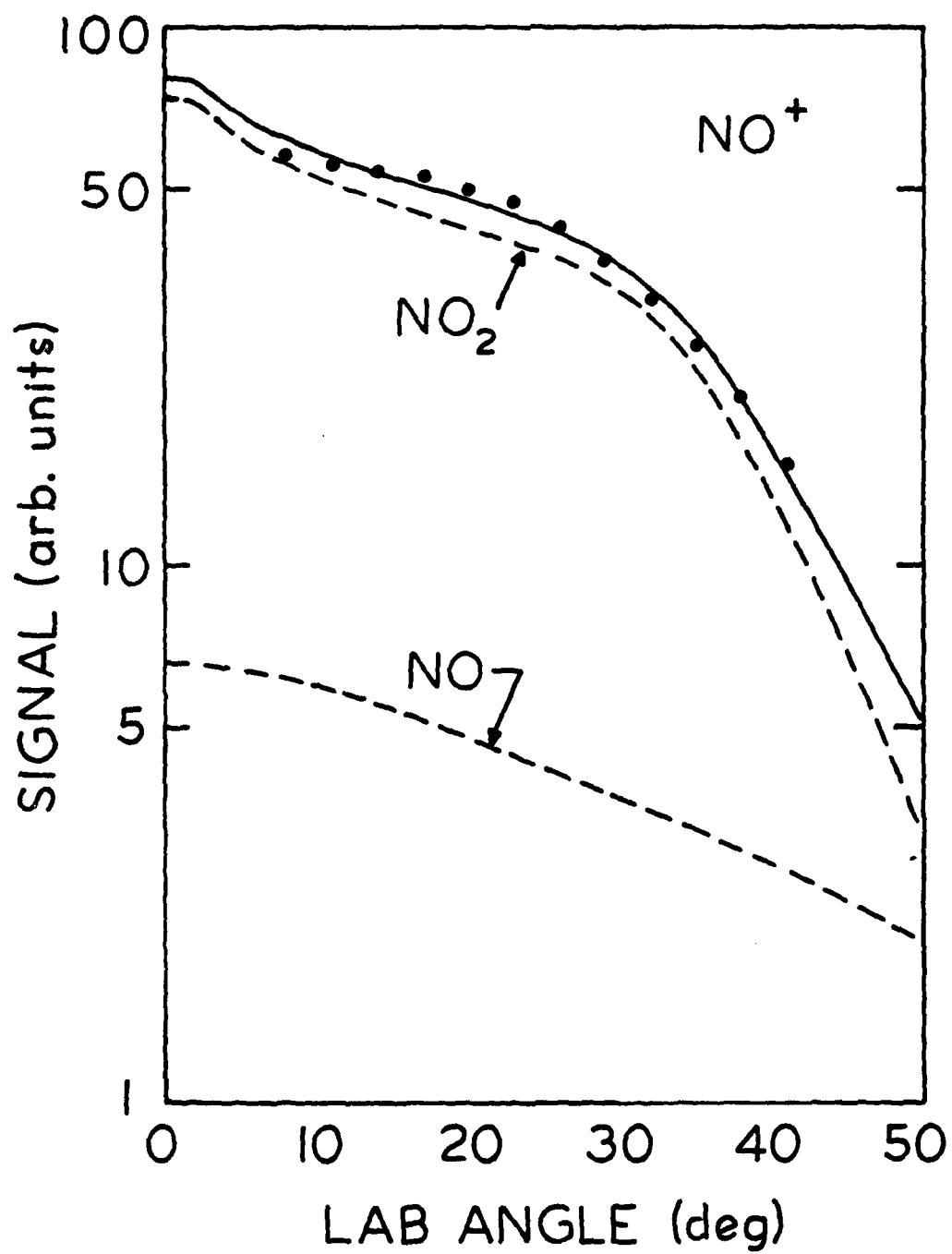
XBL 832-6351
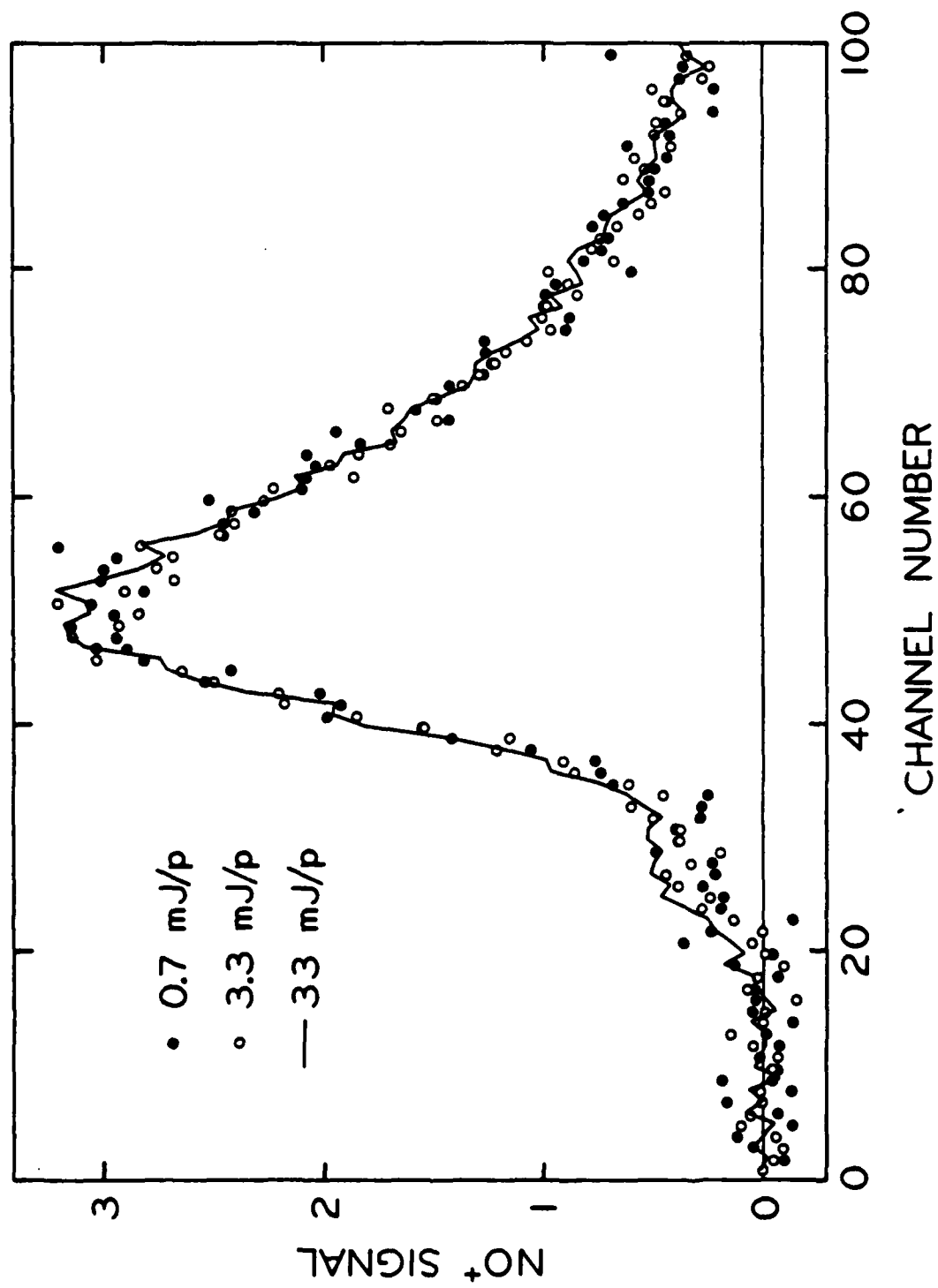
XBL 832-8291

ANGULAR DISTRIBUTION

$CH_3NO_2 \xrightarrow[nm]{193} CH_3 + NO_2^*$

$B = -.30 \pm .1$

$NO_2 \xrightarrow{h\nu} NO + O$

$P(E')$

E' (kcal / mole)
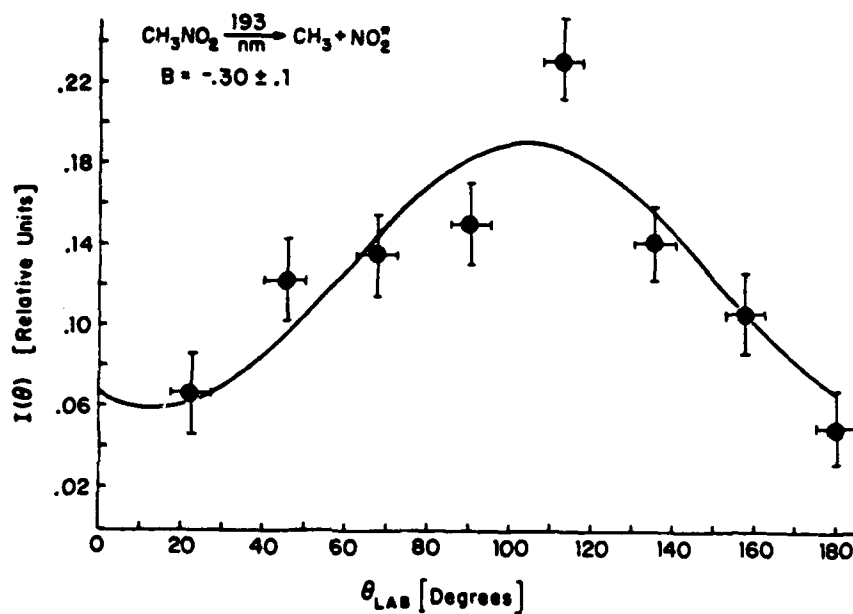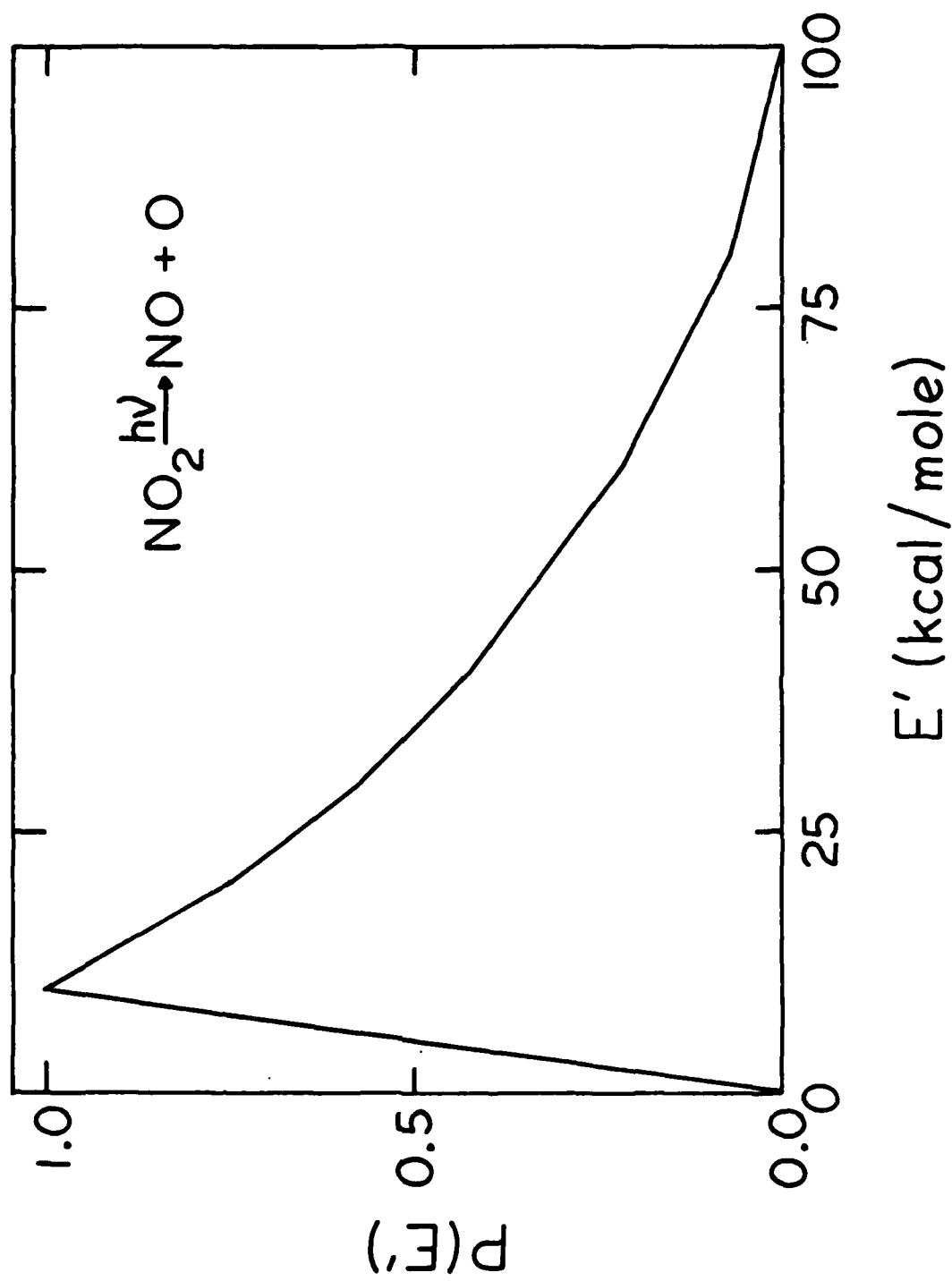
XBL 832-8192

XBL 829-11841A

XBL 832-8191

NUMBER DENSITY vs FLIGHT TIME (μsec)

$\frac{m}{e}$ = 16   10°

DEI